

## Tensor renormalization group and the volume independence in 2D $U(N)$ and $SU(N)$ gauge theories

Mitsuaki HIRASAWA<sup>1)\*</sup>, Akira MATSUMOTO<sup>1)†</sup>,  
Jun NISHIMURA<sup>1,2)‡</sup> and Atis YOSPRAKOB<sup>1)§</sup>

<sup>1)</sup>*Department of Particle and Nuclear Physics,  
School of High Energy Accelerator Science,  
Graduate University for Advanced Studies (SOKENDAI),  
1-1 Oho, Tsukuba, Ibaraki 305-0801, Japan*

<sup>2)</sup>*KEK Theory Center, Institute of Particle and Nuclear Studies,  
High Energy Accelerator Research Organization,  
1-1 Oho, Tsukuba, Ibaraki 305-0801, Japan*

### Abstract

The tensor renormalization group method is a promising approach to lattice field theories, which is free from the sign problem unlike standard Monte Carlo methods. One of the remaining issues is the application to gauge theories, which is so far limited to  $U(1)$  and  $SU(2)$  gauge groups. In the case of higher rank, it becomes highly nontrivial to restrict the number of representations in the character expansion to be used in constructing the fundamental tensor. We propose a practical strategy to accomplish this and demonstrate it in 2D  $U(N)$  and  $SU(N)$  gauge theories, which are exactly solvable. Using this strategy, we obtain the singular-value spectrum of the fundamental tensor, which turns out to have a definite profile in the large- $N$  limit. For the  $U(N)$  case, in particular, we show that the large- $N$  behavior of the singular-value spectrum changes qualitatively at the critical coupling of the Gross-Witten-Wadia phase transition. As an interesting consequence, we find a new type of volume independence in the large- $N$  limit of the 2D  $U(N)$  gauge theory with the  $\theta$  term in the strong coupling phase, which goes beyond the Eguchi-Kawai reduction.

---

\*E-mail address : mitsuaki@post.kek.jp

†E-mail address : akiram@post.kek.jp

‡E-mail address : jnishi@post.kek.jp

§E-mail address : ayosp@post.kek.jp

# 1 Introduction

Recently the tensor renormalization group method (TRG) has attracted a lot of attention as a new method to investigate lattice field theories [1]. In particular, it is totally free from the notorious sign problem due to its non-stochastic nature unlike conventional Monte Carlo methods. Another remarkable feature of the method is its accessibility to the infinite volume limit; the computational cost grows only logarithmically with the lattice size as opposed to Monte Carlo methods whose cost grows at least linearly. This owes to the efficient coarse-graining procedure reminiscent of the renormalization group based on the singular-value decomposition of the fundamental tensor.

The method was originally applied to the 2D Ising model [1], and it was extended to other spin models [2, 3, 4, 5] and theories with continuous variables such as scalar field theories [6, 7]. As yet another notable feature of the TRG, it allows direct implementation of fermionic degrees of freedom as Grassmann variables [8, 9, 10, 11, 12, 13, 14, 15, 16, 17, 18] unlike in Monte Carlo methods, which inevitably require some sort of “bosonization” leading to huge increase in the computational cost. While extension to higher dimensional theories is not as straightforward as in Monte Carlo methods, there are various proposals for efficient schemes to construct a coarse-grained tensor network [19, 20], which have been successfully applied to simple four-dimensional theories [21, 22, 23].

One of the remaining issues in the TRG is the application to gauge theories, which is so far limited to  $U(1)$  and  $SU(2)$  gauge groups [24, 25, 26, 27]. In view of this situation, here we discuss its application to  $U(N)$  and  $SU(N)$  gauge theories using the character expansion to rewrite the group integral as a sum over discrete indices. Unlike in  $U(1)$  and  $SU(2)$  gauge theories, it is highly nontrivial to restrict the number of representations to be used in constructing the fundamental tensor. We propose a practical strategy to accomplish this, and apply it to the 2D case, which is exactly solvable [28, 29, 30]. It turns out that all the procedures for the TRG can be worked out explicitly. Using the proposed strategy for restricting the number of representations, we are able to obtain the singular-value spectrum efficiently. We find, in particular, that the singular-value spectrum of the fundamental tensor thus obtained has a definite profile in the large- $N$  limit. Based on this fact, we propose a novel interpretation of the volume independence in the large- $N$  limit known as the Eguchi-Kawai reduction [31] in terms of the tensor renormalization group.

We also discuss how the expectation values of the observables depend on the cutoff  $D_{\text{cut}}$  in the singular-value spectrum. In particular, we show that the finite  $D_{\text{cut}}$  effects become severe for small  $N$ , small volume and at weak coupling. The proposed strategy enables us to obtain explicit results even in such cases. We show how the well-known Gross-

Witten-Wadia third-order phase transition [28, 29] appears as  $N$  is increased. We also obtain explicit results for the  $U(N)$  gauge theory with the  $\theta$  term, which are inaccessible to standard Monte Carlo methods due to the severe sign problem. We show how the first-order phase transition at  $\theta = \pi$  associated with the spontaneous breaking of parity symmetry appears as the volume is increased. Moreover, we find a new type of volume independence in the large- $N$  limit of the 2D  $U(N)$  gauge theory with the  $\theta$  term in the strong coupling phase, which goes beyond the Eguchi-Kawai reduction. We provide a theoretical understanding of this property by investigating the large- $N$  behavior of the singular-value spectrum in the presence of the  $\theta$  term.

The rest of this paper is organized as follows. In Section 2, we define  $U(N)$  and  $SU(N)$  lattice gauge theories in two dimensions, and construct the fundamental tensor for the TRG. In Section 3, we briefly review the TRG in 2D and explain, in particular, the coarse-graining procedure. In Section 4, we propose a practical strategy to restrict the number of representations to be used in constructing the fundamental tensor. We obtain the singular-value spectrum of the fundamental tensor, and discuss the large- $N$  behavior and its implications including the novel interpretation of the Eguchi-Kawai reduction. In Section 5, we present explicit results for observables at finite  $N$  and finite volume. We discuss how the Gross-Witten-Wadia third-order phase transition appears as  $N$  is increased. In Section 6, we investigate 2D  $U(N)$  gauge theory with the  $\theta$  term, and show how the first-order phase transition appears as the volume is increased. We also discuss the new type of volume independence in the large- $N$  limit in the strong coupling phase, which goes beyond the Eguchi-Kawai reduction. Section 7 is devoted to a summary and discussions. In appendix A, we prove a mathematical statement about the dimensionality of irreducible representations, which plays a crucial role in our strategy for restricting the number of representations.

**Note added.** When this paper was about to be completed, we encountered a preprint [32] on the arXiv, in which the TRG is applied to the  $SU(2)$  and  $SU(3)$  gauge theories in 2D without using the character expansion. The fundamental tensor is made finite-dimensional by replacing the group integral by a sum over a finite number of randomly chosen  $SU(N)$  matrices analogously to how the scalar field theories are dealt with in the TRG. In this method, it is easier to introduce the matter fields although it is hard to go to larger  $N$ .

## 2 Tensor network representation of 2D gauge theory

In this section, we consider the 2D  $U(N)$  and  $SU(N)$  gauge theories and rewrite the partition function in the tensor network representation. In the continuum, the action is given by

$$S = \frac{1}{4g^2} \int d^2x \operatorname{tr}(F_{\mu\nu})^2, \quad (2.1)$$

where  $F_{\mu\nu}$  is the field strength tensor

$$F_{\mu\nu} = \partial_\mu A_\nu - \partial_\nu A_\mu - i[A_\mu, A_\nu] \quad (2.2)$$

defined with the gauge field  $A_\mu$ .

In order to put the theory on a lattice, we introduce discrete spacetime points  $x^\mu = an^\mu$  labeled by the integer vector  $n^\mu$  with a lattice spacing  $a$ . We define the link variable  $U_{n,\mu} \in U(N)$  or  $SU(N)$ , which corresponds to the gauge field as  $U_{n,\mu} \sim \exp(iaA_\mu(x))$ , and consider the action

$$S = -\frac{N}{\lambda} \sum_n \operatorname{tr}(P_n + P_n^\dagger), \quad (2.3)$$

where we have defined the plaquette

$$P_n = U_{n,1} U_{n+1,2} U_{n+2,1}^\dagger U_{n,2}^\dagger \quad (2.4)$$

and the dimensionless 't Hooft coupling constant  $\lambda = 2Ng^2a^2$ , which is fixed when we take the  $N \rightarrow \infty$  limit for fixed  $a$ . In the continuum limit  $a \rightarrow 0$  with fixed  $g^2N$ , one retrieves the action (2.1) in the continuum. The partition function of the lattice theory is given as

$$Z = \int DU e^{-S}, \quad (2.5)$$

where  $DU$  represents the Haar measure for the link variables. The 2D lattice gauge theory is exactly solvable as demonstrated first in the infinite-volume limit [28, 29], and later also for finite volume [30]. Below we review the evaluation of the partition function using the character expansion method [33, 34, 35].

The first step of the character expansion is to rewrite the Boltzmann weight  $e^{-S}$  in (2.5) as a product of functions of each plaquette  $P_n$ ,

$$e^{-S} = \prod_n f(P_n), \quad (2.6)$$

$$f(P) = \exp \left\{ \frac{N}{\lambda} \operatorname{tr}(P + P^\dagger) \right\}. \quad (2.7)$$

The function  $f(P)$  has a special property

$$f(P) = f(g^{-1}Pg) , \quad \forall g \in \text{U}(N) \text{ or } \text{SU}(N) , \quad (2.8)$$

which allows the so-called character expansion

$$f(P) = \sum_r \tilde{\beta}_r \text{tr}_r(P) , \quad (2.9)$$

where the sum is taken over all the irreducible representations<sup>1</sup> of the gauge group and the symbol  $\text{tr}_r$  implies that the trace is taken with respect to the representation  $r$ . The coefficient  $\tilde{\beta}_r$  of the expansion can be evaluated as

$$\tilde{\beta}_r = \int dU f(U) \text{tr}_r(U^\dagger) . \quad (2.10)$$

Substituting (2.7) into (2.10), one obtains [36]

$$\tilde{\beta}_r = \begin{cases} \det \mathcal{M}_{r,0} & \text{for } \text{U}(N) , \\ \sum_{q \in \mathbb{Z}} \det \mathcal{M}_{r,q} & \text{for } \text{SU}(N) . \end{cases} \quad (2.11)$$

The matrix  $\mathcal{M}_{r,q}$  is defined by

$$\left( \mathcal{M}_{r,q} \right)_{ij} = \int_{-\pi}^{+\pi} \frac{d\phi}{2\pi} \cos\{(l_j + i - j + q)\phi\} \exp\left(\frac{2N}{\lambda} \cos \phi\right) = I_{l_j+i-j+q}\left(\frac{2N}{\lambda}\right) \quad (2.12)$$

for  $i, j = 1, 2, \dots, N$ , where  $I_n(x)$  is the modified Bessel function of the first kind. Here we have labeled the representation  $r$  by a set of  $N$  integers  $\{l_1, \dots, l_N\}$  satisfying

$$l_1 \geq l_2 \geq \dots \geq l_N \quad (2.13)$$

with an extra constraint  $l_N = 0$  in the  $\text{SU}(N)$  case, where the label  $\{l_i\}$  is commonly represented by the Young tableau with  $l_i$  boxes in the  $i$ th row. The dimensionality of a representation  $r = \{l_i\}$  for either gauge group is given by

$$d_r = \prod_{1 \leq i < j \leq N} \left(1 + \frac{l_i - l_j}{j - i}\right) . \quad (2.14)$$

Note that any representation  $r^{(\text{U})} = \{l'_i\}$  of  $\text{U}(N)$  can be obtained uniquely from a representation  $r^{(\text{SU})} = \{l_i\}$  of  $\text{SU}(N)$  by

$$l'_i = l_i + q \quad (2.15)$$

---

<sup>1</sup>In what follows, we refer to irreducible representations simply as representations.

with some integer  $q$ . According to the definition of the label  $\{l_i\}$ , the representation matrix  $D^{r^{(U)}}(g)$  of  $g \in U(N)$  for the representation  $r^{(U)}$  is given by

$$D^{r^{(U)}}(g) = e^{ip\theta} D^{r^{(\text{SU})}}(\tilde{g}) , \quad (2.16)$$

$$p \equiv \sum_{i=1}^N l'_i = \sum_{i=1}^{N-1} l_i + Nq , \quad (2.17)$$

where  $D^{r^{(\text{SU})}}(\tilde{g})$  is the representation matrix of  $\tilde{g} \in \text{SU}(N)$  for the representation  $r^{(\text{SU})}$  and  $g = e^{i\theta}\tilde{g}$ . The right-hand side of (2.16) is invariant under  $\tilde{g} \mapsto e^{\frac{2\pi ik}{N}}\tilde{g} \in \text{SU}(N)$  and  $\theta \mapsto \theta - \frac{2\pi k}{N}$  ( $k \in \mathbf{Z}$ ) since

$$D^{r^{(\text{SU})}}(e^{\frac{2\pi ik}{N}}\tilde{g}) = e^{\frac{2\pi ik}{N}\sum l_i} D^{r^{(\text{SU})}}(\tilde{g}) . \quad (2.18)$$

In what follows, we use the notation

$$\begin{aligned} \text{trv}^{(U)} &= \{0, 0, \dots, 0, 0\} , & \text{trv}^{(\text{SU})} &= \{0, 0, \dots, 0, 0\} , \\ \text{fnd}^{(U)} &= \{1, 0, \dots, 0, 0\} , & \text{fnd}^{(\text{SU})} &= \{1, 0, \dots, 0, 0\} , \\ \overline{\text{fnd}}^{(U)} &= \{0, 0, \dots, 0, -1\} , & \overline{\text{fnd}}^{(\text{SU})} &= \{1, 1, \dots, 1, 0\} , \\ \text{adj}^{(U)} &= \{1, 0, \dots, 0, -1\} , & \text{adj}^{(\text{SU})} &= \{2, 1, \dots, 1, 0\} , \end{aligned} \quad (2.19)$$

where ‘‘trv’’, ‘‘fnd’’ and ‘‘adj’’ are abbreviation for the trivial, fundamental and adjoint representations, respectively, and the bar like the one in ‘‘ $\overline{\text{fnd}}$ ’’ above implies the complex conjugate representation.

Using the character expansion, the partition function becomes

$$Z = \int DU \prod_n f(P_n) = \sum_{\{r(n)\}} \int DU \prod_n \tilde{\beta}_{r(n)}^{\text{tr}_{r(n)}(P_n)} , \quad (2.20)$$

where  $r(n)$  is the representation that appears in the character expansion of  $f(P_n)$ . Next we decompose  $\text{tr}_{r(n)}(P_n)$  in terms of link variables as

$$\text{tr}_{r(n)}(P_n) = D_{\alpha\beta}^{r(n)}(U_{n,1}) D_{\beta\gamma}^{r(n)}(U_{n+1,2}) D_{\gamma\delta}^{r(n)}(U_{n+2,1}^\dagger) D_{\delta\alpha}^{r(n)}(U_{n,2}^\dagger) , \quad (2.21)$$

where  $D^r(U)$  is the representation matrix of  $U$  for the representation  $r$ , and the indices  $\alpha, \beta, \gamma, \delta$  are summed over implicitly. It can then be seen<sup>2</sup> that any given link variable  $U_{n,\mu}$  appears only twice in (2.20); one as  $U$  and the other as  $U^\dagger$ . Therefore, the partition

---

<sup>2</sup>Note that this is the case only in two dimensions.

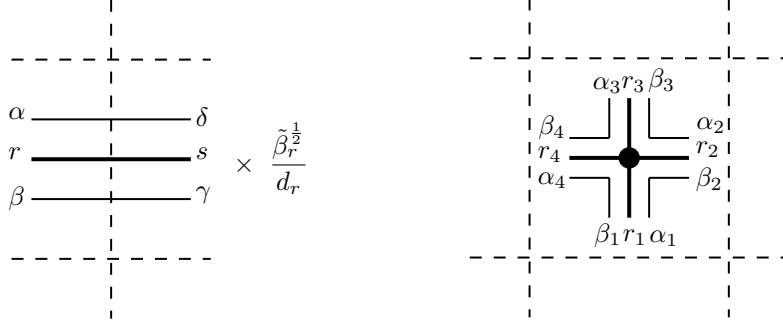


Figure 1: The tensor associated with each link (Left) and that associated with each plaquette (Right) are depicted corresponding to (2.23) and (2.25), respectively.

function factorizes into the integral for each link variable as

$$Z = \prod_{n,\mu} z^{(n,\mu)} , \quad (2.22)$$

$$(z^{(n,\mu)})_{rs\alpha\beta\gamma\delta} = \tilde{\beta}_r^{\frac{1}{4}} \tilde{\beta}_s^{\frac{1}{4}} \int dU_{n,\mu} D_{\alpha\beta}^r(U_{n,\mu}) D_{\gamma\delta}^s(U_{n,\mu}^\dagger) = \frac{\tilde{\beta}_r^{\frac{1}{2}}}{d_r} \delta_{rs} \delta_{\alpha\delta} \delta_{\beta\gamma} , \quad (2.23)$$

where we have used the orthogonality relation

$$\int dU D_{\alpha\beta}^r(U) D_{\gamma\delta}^s(U^\dagger) = \frac{1}{d_r} \delta_{rs} \delta_{\alpha\delta} \delta_{\beta\gamma} \quad (2.24)$$

with  $d_r$  being the dimensionality of the representation  $r = \{l_i\}$  given by (2.14).

The tensor (2.23) can be considered to be associated with each link on the lattice as depicted in Fig. 1 (Left). Note also that on the right-hand side of (2.22), the indices of  $(z^{(n,\mu)})_{rs\alpha\beta\gamma\delta}$  are assumed to be contracted appropriately according to (2.21). As a result, we also have a tensor

$$\delta_{r_1 r_2 r_3 r_4} \delta_{\alpha_1 \beta_2} \delta_{\alpha_2 \beta_3} \delta_{\alpha_3 \beta_4} \delta_{\alpha_4 \beta_1} \quad (2.25)$$

associated with each plaquette as depicted in Fig. 1 (Right), where we have defined

$$\delta_{r_1 r_2 r_3 r_4} = \begin{cases} 1 & \text{for } r_1 = \dots = r_4 , \\ 0 & \text{otherwise.} \end{cases} \quad (2.26)$$

Note that the matrix indices form a loop around each site yielding a factor of  $d_r$  for each site. Thus we end up with a tensor network

$$Z = \prod T , \quad (2.27)$$

where the fundamental tensor  $(T)_{pqrs}$  for each plaquette is defined as

$$(T)_{pqrs} = \frac{\tilde{\beta}_p}{d_p} \delta_{pqrs} , \quad (2.28)$$

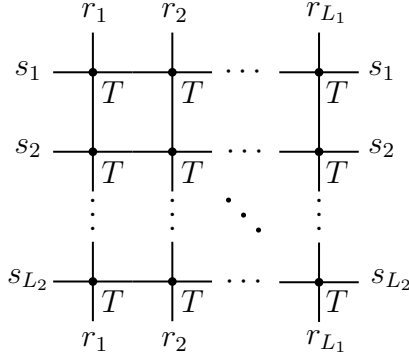


Figure 2: The tensor network representing the partition function (2.27).

after reassigning the factor  $\frac{\tilde{\beta}_r^{\frac{1}{2}}}{d_r}$  for each link to the two plaquettes sharing it and reassigning the factor  $d_r$  for the site  $n$  to the plaquette  $P_n$ . The indices of the fundamental tensor  $(T)_{pqrs}$  in (2.27) are assumed to be contracted appropriately as depicted in Fig. 2, where we impose periodic boundary conditions.

In the present case, the structure of the fundamental tensor is so simple that we can evaluate (2.27) for an  $L_1 \times L_2$  lattice as

$$Z = \sum_r \left( \frac{\tilde{\beta}_r}{d_r} \right)^{L_1 L_2}, \quad (2.29)$$

which agrees with the known exact result in Ref. [30].

### 3 Brief review of the TRG in 2D

In this section we briefly review the TRG [1], which is a useful method that can be applied to various theories whose partition function is written as a network of tensors with translational invariance. The crucial point is to make use of the coarse graining to access a large system size efficiently. Here we explain the method in 2D.

The TRG consists of two steps. The first step is to decompose the tensor  $T$  using the singular-value decomposition (SVD). Let us consider the following two types of SVD. The first one amounts to regarding the double indices  $(q, r)$  and  $(s, p)$  of the tensor  $T_{pqrs}$  as single indices  $a$  and  $b$ , respectively, and applying the SVD to the resulting matrix with the two indices  $a$  and  $b$  as

$$T_{pqrs} = \sum_c S_{ac}^{(1)} G_c^{(1)} S_{cb}^{(2)} = \sum_c \tilde{S}_{ac}^{(1)} \tilde{S}_{cb}^{(2)}, \quad (3.1)$$



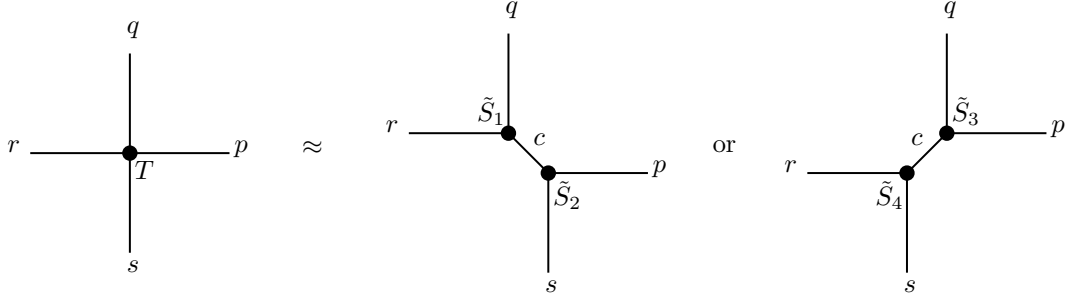


Figure 3: The two types of SVD used for even sites and odd sites, respectively.

where  $S^{(1)}$  and  $S^{(2)}$  are unitary matrices and  $G_c^{(1)}$  are the singular values, which are positive-semidefinite and labeled in the descending order. In the second equality, we have absorbed the singular values into the  $S^{(1)}$  and  $S^{(2)}$  as

$$\tilde{S}_{ac}^{(1)} = S_{ac}^{(1)} \sqrt{G_c^{(1)}}, \quad \tilde{S}_{cb}^{(2)} = S_{cb}^{(2)} \sqrt{G_c^{(1)}}. \quad (3.2)$$

Similarly, we define the second type of SVD by regarding the double indices  $(p, q)$  and  $(r, s)$  of the tensor  $T_{pqrs}$  as single indices  $a$  and  $b$ , respectively, and applying the SVD to the resulting matrix with the two indices  $a$  and  $b$  as

$$T_{pqrs} = \sum_c S_{ac}^{(3)} G_c^{(2)} S_{cb}^{(4)} = \sum_c \tilde{S}_{ac}^{(3)} \tilde{S}_{cb}^{(4)}, \quad (3.3)$$

where  $S^{(3)}$ ,  $S^{(4)}$  are unitary matrices and  $G_c^{(2)}$  are the singular values, which are again positive-semidefinite and labeled in the descending order. In the second equality, we have absorbed the singular values into the  $S^{(3)}$  and  $S^{(4)}$  as

$$\tilde{S}_{ac}^{(3)} = S_{ac}^{(3)} \sqrt{G_c^{(2)}}, \quad \tilde{S}_{cb}^{(4)} = S_{cb}^{(4)} \sqrt{G_c^{(2)}}. \quad (3.4)$$

The two types of SVD (3.1) and (3.3) can be represented diagrammatically as in Fig. 3. We apply them on the even and odd sites of the lattice, respectively<sup>3</sup>, which is shown in Fig. 4 as the first step from the left to the middle.

The second step is to define

$$T'_{abcd} = \sum_{pqrs} \tilde{S}_{(q,r),a}^{(1)} \tilde{S}_{(r,s),d}^{(3)} \tilde{S}_{c,(s,p)}^{(2)} \tilde{S}_{b,(p,q)}^{(4)}, \quad (3.5)$$

which represents the coarse-grained version of the original tensor  $T_{pqrs}$ . This is shown in Fig. 4 as the second step from the middle to the right. Note that the new lattice is

<sup>3</sup>Here we need to assume that the number of sites in each direction is even in order to assign the parity to each site consistently to the boundary condition.

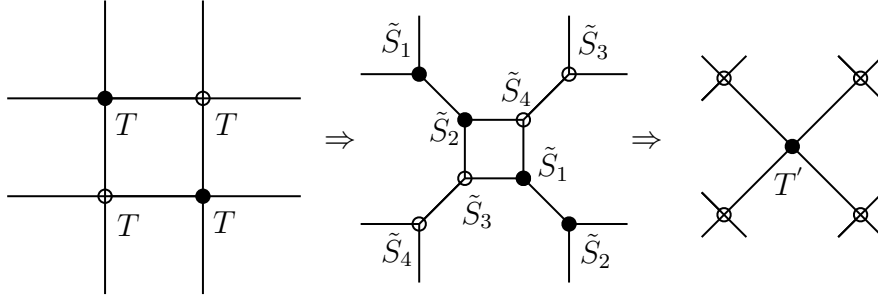


Figure 4: The two steps in the coarse-graining procedure for the tensor network.

tilted by  $45^\circ$  degrees, but the boundary condition is such that it respects the translational invariance in the directions of the original lattice. Repeating this procedure twice, one obtains a  $L/2 \times L/2$  lattice with periodic boundary conditions. Thus, starting from a  $2^n \times 2^n$  lattice, we can perform the coarse graining  $2n$  times to arrive at a one-site model with the fundamental tensor  $T''_{pqrs}$ , whose partition function can be evaluated as

$$Z = \sum_{p,q} T''_{pqpq} . \quad (3.6)$$

In general, the fundamental tensor has a form more complicated than (2.28), and the SVD such as (3.1), (3.3) has to be done numerically. Note also that an index of the coarse-grained version of the fundamental tensor corresponds to the double indices of the original one as we discussed above. Therefore, one needs to truncate the range of the indices in order to avoid the growth of the numerical cost as the coarse graining proceeds. The crucial point of the TRG is to perform this truncation by keeping only the large singular values in the expressions like (3.1) and (3.3). Thus the fundamental tensor has indices with the same dimension, which is called the bond dimension  $D_{\text{cut}}$ , throughout the coarse-graining procedure. One has to increase  $D_{\text{cut}}$  until the results do not change any more. The required value of  $D_{\text{cut}}$  is basically determined by the fall-off of the singular-value spectrum, which becomes slow as the correlation length of the theory increases. The numerical cost of the TRG grows proportionally to  $D_{\text{cut}}^n$  with some power  $n$ , which is 6 in the 2D case and becomes larger for theories in higher dimensions. Recently, some new TRG schemes [4, 19, 20] for higher dimensional models have been proposed to reduce the power  $n$  considerably.

## 4 Application to $U(N)$ and $SU(N)$ gauge theories

When one applies the TRG to a gauge theory with a continuous group using the character expansion, the dimension of the original fundamental tensor is infinite because there are

infinitely many representations. In the case of  $U(1)$  and  $SU(2)$  gauge groups, which have been studied so far in the literature [24, 25, 26, 27], there is a natural choice for restricting the number of representations because the representation is labeled by the charge and the spin, respectively. Obviously, this issue becomes more nontrivial in the case of  $SU(N)$  and  $U(N)$  gauge groups with  $N \geq 3$ .

In the 2D lattice gauge theory that we are considering, the fundamental tensor takes a particularly simple form (2.28), and one can obtain the product (2.27) exactly to arrive at the well-known result (2.29). However, one still has to truncate the summation over representations in (2.29) in order to obtain explicit results in general.

Here we discuss how we can restrict the number of representations to be included in the fundamental tensor efficiently so that the singular-value spectrum is correctly reproduced up to a given bond dimension  $D_{\text{cut}}$ . Then, we discuss various properties of the singular-value spectrum, in particular, at large  $N$ , and consider their implications.

## 4.1 singular-value spectrum in the 2D gauge theories

In the case of 2D lattice gauge theory, the fundamental tensor is given by (2.28), which allows us to make the SVD trivially. Namely, for the two types of SVD, the singular values  $G_{(r,s)}^{(i)}$  ( $i = 1, 2$ ) are given by

$$G_{(r,s)}^{(i)} = \sigma_r \delta_{rs} , \quad \sigma_r \equiv \frac{|\tilde{\beta}_r|}{d_r} . \quad (4.1)$$

One can easily find that the coarse-grained tensor (3.5) becomes

$$T'_{pqrs} = (\sigma_p)^2 \delta_{pqrs} , \quad (4.2)$$

which has the same form as (2.28). Repeating this procedure  $2n$  times starting with a system on the  $L \times L$  lattice, where  $L = 2^n$ , one obtains a one-site model with the fundamental tensor

$$T''_{pqrs} = (\sigma_p)^V \delta_{pqrs} , \quad (4.3)$$

where  $V = L^2$  is the volume of the lattice. Plugging this into (3.6), the partition function is given in terms of the singular values  $\sigma_r$  as

$$Z = \sum_r (\sigma_r)^V , \quad (4.4)$$

which agrees with the exact result (2.29). Thus, the TRG can be worked out explicitly in this model, and the only remaining task is to determine the largest  $D_{\text{cut}}$  singular values of the fundamental tensor.

Due to the simple  $V$ -dependence of the partition function, one finds in the infinite-volume limit  $V \rightarrow \infty$  that the summation in (4.4) is dominated by the largest singular value, which is known to correspond to the trivial representation,

$$\sigma_{\text{trv}} = \int dU \exp \left\{ \frac{N}{\lambda} \text{tr}(U + U^\dagger) \right\}, \quad (4.5)$$

where we have used (2.10) and (2.7). The right-hand side of (4.5) is nothing but the partition function of the one-plaquette model obtained in the  $V \rightarrow \infty$  limit of 2D lattice gauge theory [28, 29], and in the large- $N$  limit, one obtains

$$C^{(0)} \equiv \lim_{N \rightarrow \infty} \frac{1}{N^2} \log \sigma_{\text{trv}} = \begin{cases} \frac{2}{\lambda} + \frac{1}{2} \log \frac{\lambda}{2} - \frac{3}{4} & \text{for } \lambda < 2, \\ \frac{1}{\lambda^2} & \text{for } \lambda \geq 2 \end{cases}, \quad (4.6)$$

for both  $SU(N)$  and  $U(N)$  gauge theories. Let us emphasize, however, that this simplification in the  $V \rightarrow \infty$  limit is peculiar to the present 2D gauge theories. The change of the behavior at  $\lambda = 2$  in (4.6) indicates the Gross-Witten-Wadia phase transition, which plays an important role in what follows.

## 4.2 restricting the number of representations

Here we discuss how to restrict the number of representations in the case of  $SU(N)$  and  $U(N)$  gauge groups, which is nontrivial since the representations are labeled by more than one parameters  $\{l_i\}$ . As a natural requirement, the cutoff scheme should not discriminate representations which are complex conjugate to each other. We will consider three cutoff schemes which satisfy this requirement and discuss which is the most efficient.

Let us first consider the  $SU(N)$  case. As is mentioned in Section 2, the representations of  $SU(N)$  are parametrized by  $(N - 1)$  non-negative integers  $l_1, l_2, \dots, l_{N-1}$  satisfying

$$l_1 \geq l_2 \geq \dots \geq l_{N-1} \geq l_N = 0. \quad (4.7)$$

Considering that the complex conjugate representation of  $\{l_i\}$  is given by  $\{\bar{l}_i\}$ , where  $\bar{l}_i = l_1 - l_{N+1-i}$ , we have  $\bar{l}_1 = l_1$ . In view of this, a simple choice would be to introduce a cutoff  $l_1 \leq \Lambda$ , where  $\Lambda$  is some integer. The number of representations within this cutoff can be shown<sup>4</sup> to be  ${}_{\Lambda+N-1}C_\Lambda$ , which grows as  $\Lambda^{N-1}$  with  $\Lambda$  for fixed  $N$ .

<sup>4</sup>Let us introduce integers  $n_1, \dots, n_N \geq 0$  through  $l_1 = \Lambda - n_1$  and  $l_{i+1} = l_i - n_{i+1}$  ( $i = 1, \dots, N - 1$ ), which implies  $l_N = \Lambda - \sum_{j=1}^N n_j$ . Imposing  $l_N = 0$ , we get the relation  $\sum_{j=1}^N n_j = \Lambda$ . Thus, the issue of counting the representations with  $l_1 \leq \Lambda$  reduces to that of assigning  $\Lambda$  identical objects into  $N$  partitions.

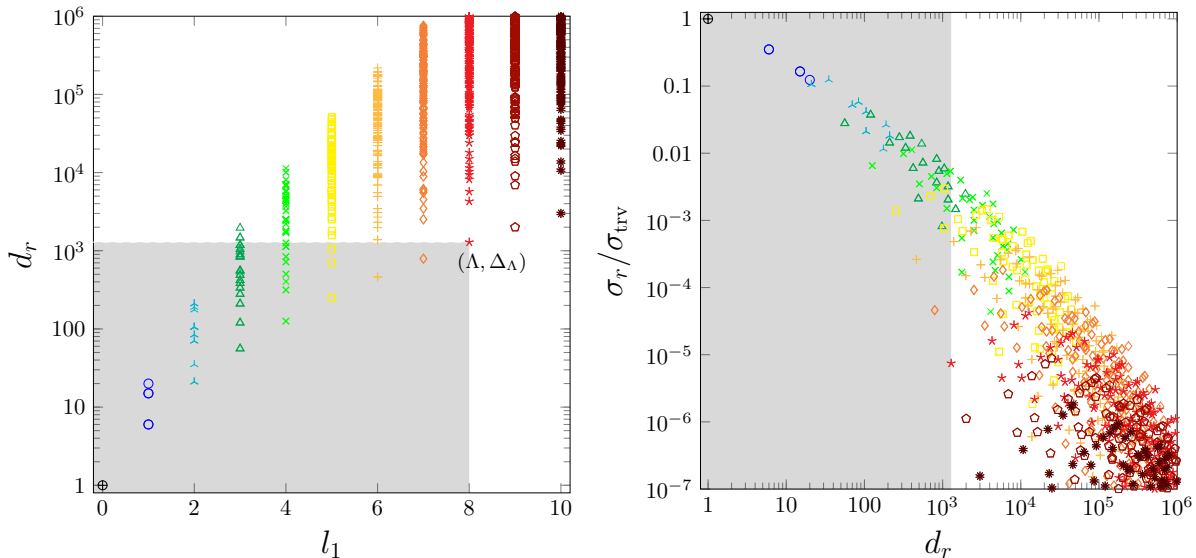


Figure 5: (Left) The dimensionality of the representations of the SU(6) group is plotted against  $l_1$ . The shaded region corresponds to  $d_r \leq \Delta_\Lambda$  and  $l_1 \leq \Lambda$  with  $\Lambda = 8$ . (Right) The singular value  $\sigma_r$  normalized by  $\sigma_{\text{trv}}$  is plotted against the dimensionality for the SU(6) gauge theory with  $\lambda = 3$ . Different symbols correspond to different  $l_1$  as shown in the left panel. The shaded region corresponds to  $d_r \leq \Delta_\Lambda$  with  $\Lambda = 8$ .

Another possibility is to put an upper bound on the dimensionality (2.14) of the representation, which is obviously the same for the complex conjugate pairs. In Fig. 5 (Left), we plot the dimensionality  $d_r$  of each representation  $r$  of the SU(6) group against  $l_1$ . Let us note here that the representation of the SU( $N$ ) group that has the smallest dimensionality among those with the same  $l_1 = \Lambda$  is given by the totally symmetric representation and its conjugate, which correspond to  $r = \{\Lambda, 0, \dots, 0\}$  and  $\bar{r} = \{\Lambda, \dots, \Lambda, 0\}$ , respectively. (See appendix A for a proof.) From (2.14), one finds that the dimensionality of these representations is

$$\Delta_\Lambda = \prod_{j=2}^N \left( 1 + \frac{\Lambda}{j-N} \right) = {}_{\Lambda+N-1}C_\Lambda, \quad (4.8)$$

which grows monotonically with  $\Lambda$ . Therefore, as a convenient way to put a cutoff on the dimensionality, we use  $d_r \leq \Delta_\Lambda$ , which automatically implies  $l_1 \leq \Lambda$  as is shown by the shaded region in Fig. 5 (Left) for  $\Lambda = 8$  in the SU(6) case. This makes it easy to list all the representations below the cutoff.

In Fig. 5 (Right), we plot the singular value  $\sigma_r = |\tilde{\beta}_r/d_r|$  of the fundamental tensor for  $\lambda = 3$  corresponding to each representation  $r$  against the dimensionality  $d_r$ . Different

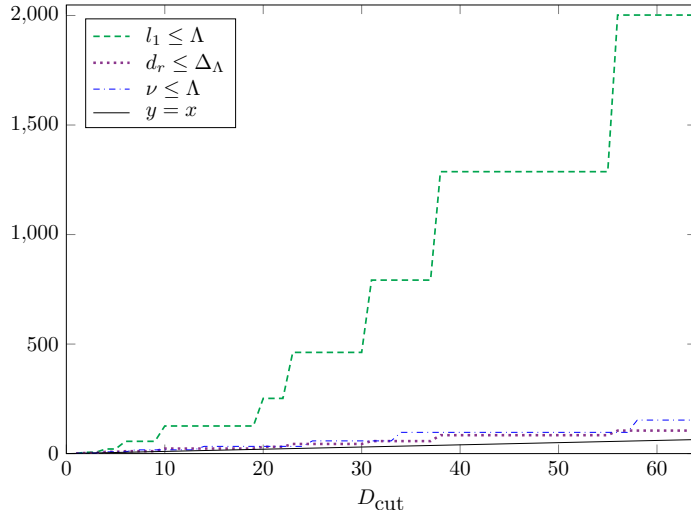


Figure 6: The number of representations required for a given  $D_{\text{cut}}$  is plotted against  $D_{\text{cut}}$  for the SU(6) gauge theory with  $\lambda = 3$ . The dashed, dotted and dash-dotted lines represent the results for the truncation by  $l_1$ , the dimensionality  $d_r$ , and  $\nu \equiv \min_{q \in \mathbb{Z}} \sum_{i=1}^N |l_i + q|$ , respectively. The solid line  $y = x$  corresponds the theoretical lower bound.

symbols correspond to different  $l_1$  as shown in the left panel. We observe a clear tendency that the singular value becomes small as either  $l_1$  or the dimensionality becomes large.

In order to compare the efficiency of the two cutoff schemes, we increase the cutoff in either cutoff scheme until the largest  $D_{\text{cut}}$  singular values of the fundamental tensor do not change any more. The number of representations below the cutoff to achieve a given value of  $D_{\text{cut}}$  is plotted in Fig. 6. It is clear that the number of representations is significantly smaller for the cutoff scheme with the dimensionality. It is also worth noting that in the case of SU(2), the two cutoff schemes reduce to the truncation by spins  $S$  since  $l_1 = 2S$  and  $d_r = 2S + 1$ . What we find here is that for  $N > 2$ , it is far more efficient to truncate the representations by the dimensionality  $d_r$  than by  $l_1$ .

Next we consider the U( $N$ ) case using the relationship (2.15) to the representations of SU( $N$ ), which can be truncated in the way described above. The remaining task is to introduce a cutoff on  $q$  in (2.15). Note that the complex conjugate representation of  $\{l'_i\}$  is given by  $\{\bar{l}'_i\}$ , where  $\bar{l}'_i = -l'_{N+1-i}$ . Therefore, as a simple cutoff on  $q$  that does not discriminate the complex conjugates, we impose

$$\max_i |l'_i| = \left| q + \frac{l_1}{2} \right| + \frac{l_1}{2} \leq \Lambda_q, \quad (4.9)$$

where  $\Lambda_q$  is an integer representing the cutoff on  $q$ . Note that this is a natural generalization of the U(1) case, where we truncate the representations by the charge.

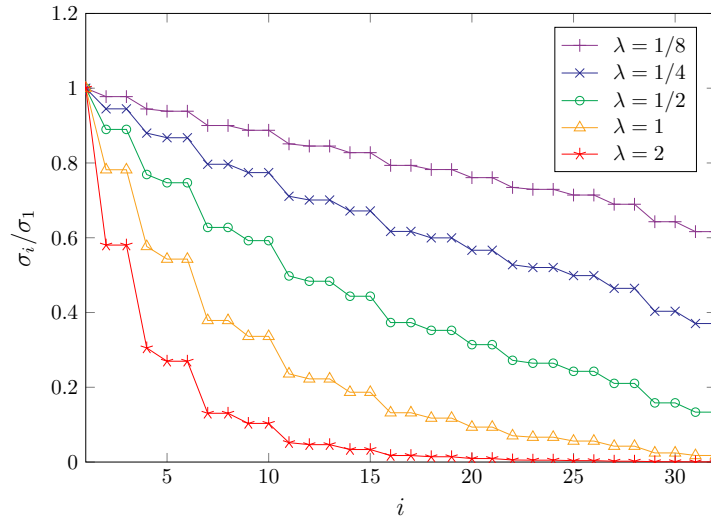


Figure 7: The singular values  $\sigma_i/\sigma_1$  ( $i = 1, 2, \dots, 32$ ) of the fundamental tensor normalized by the largest one  $\sigma_1$  are plotted in the descending order for the SU(3) gauge theory with various values of the coupling constant.

As yet another way of truncation, we can think of  $\sum_{i=1}^N |l'_i| \leq \Lambda$  for the U( $N$ ) case, which is clearly invariant under complex conjugation. The SU( $N$ ) analogue of this truncation is given by  $\nu \equiv \min_{q \in \mathbb{Z}} \sum_{i=1}^N |l_i + q| \leq \Lambda$ . The efficiency of this truncation scheme turns out to be comparable to the one with the dimensionality as we can see from Fig. 6.

### 4.3 properties of the singular-value spectrum

Using the strategy for restricting the number of representations proposed in the previous section, we can obtain the singular-value spectrum correctly up to any given  $D_{\text{cut}}$ . Below we discuss various properties of the singular-value spectrum thus obtained. First we discuss how the singular-value spectrum depends on the coupling constant. In Fig. 7, we plot the singular values  $\sigma_i$  ( $i = 1, 2, \dots$ ) sorted in the descending order for the SU(3) case with various values of the coupling constant. The singular values are normalized by the largest one  $\sigma_1$ , which corresponds to the trivial representation as we mentioned at the end of Section 4.1. We find that the singular-value spectrum falls off more slowly at weak coupling, where the correlation length becomes large.

Next we discuss the behavior of the singular values at large  $N$ . In particular, we will see that the ratio of the singular values  $\sigma_i/\sigma_1$  becomes finite in the large- $N$  limit. We also find, in the U( $N$ ) case, that the large- $N$  behavior of the singular values changes qualitatively at the critical coupling of the Gross-Witten-Wadia phase transition.

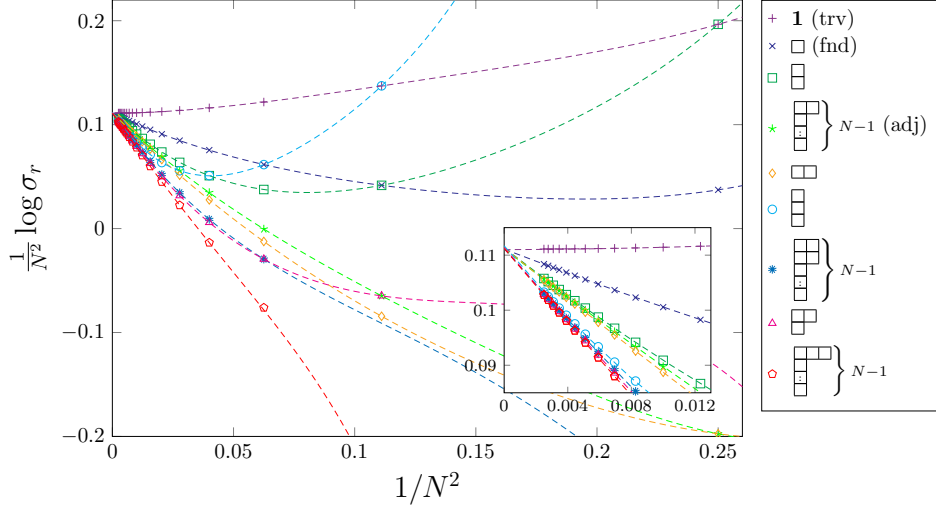


Figure 8: The singular values  $\frac{1}{N^2} \log \sigma_r$  are plotted against  $1/N^2$  for the  $SU(N)$  gauge theory with  $\lambda = 3$ . Different symbols correspond to different sequences of representations as shown on the right of the plot. Each point is actually doubly degenerate except for real representations since representations that are complex conjugate to each other give identical singular values. We restrict ourselves to the sequence of representations that correspond to the 16 largest singular values in the large- $N$  limit. The dashed lines represent fits to a quartic polynomial in  $1/N^2$  for each sequence using  $N \geq 2$ , which turn out to merge at  $C^{(0)} = \frac{1}{9}$  in the large- $N$  limit.

In order to discuss the large- $N$  behavior of the singular values, we define a sequence of representations for increasing  $N$ . For example, the trivial, (anti-)fundamental and adjoint representations, which are defined for  $N = 2, 3, \dots$  can be regarded as sequences of representations. Generalizing these examples, we define a sequence of representations, in the  $U(N)$  case, by specifying  $n \geq 0$  positive entries and  $m \geq 0$  negative entries of  $\{l'_i\}$  as

$$r^{(U)} = \{l'_1, \dots, l'_n, 0, \dots, 0, l'_{N-m+1}, \dots, l'_N\}. \quad (4.10)$$

As  $N$  increases, the number of zero entries in the middle increases while keeping the structure at both ends of  $\{l'_i\}$  fixed. By adding charge  $q \in \mathbf{Z}$  to the representations (4.10), we can obtain other sequences

$$(r^{(U)}, q) \equiv \{l'_1 + q, \dots, l'_n + q, q, \dots, q, l'_{N-m+1} + q, \dots, l'_N + q\}. \quad (4.11)$$

In the  $SU(N)$  case, we can define a sequence of representations  $r^{(SU)} \equiv \{l_i\}$ , where  $l_i = l'_i - l'_N$  ( $i = 1, \dots, N$ ), corresponding to (4.10). In what follows, we discuss the large- $N$  behavior of the singular values for the sequences of representations thus defined.



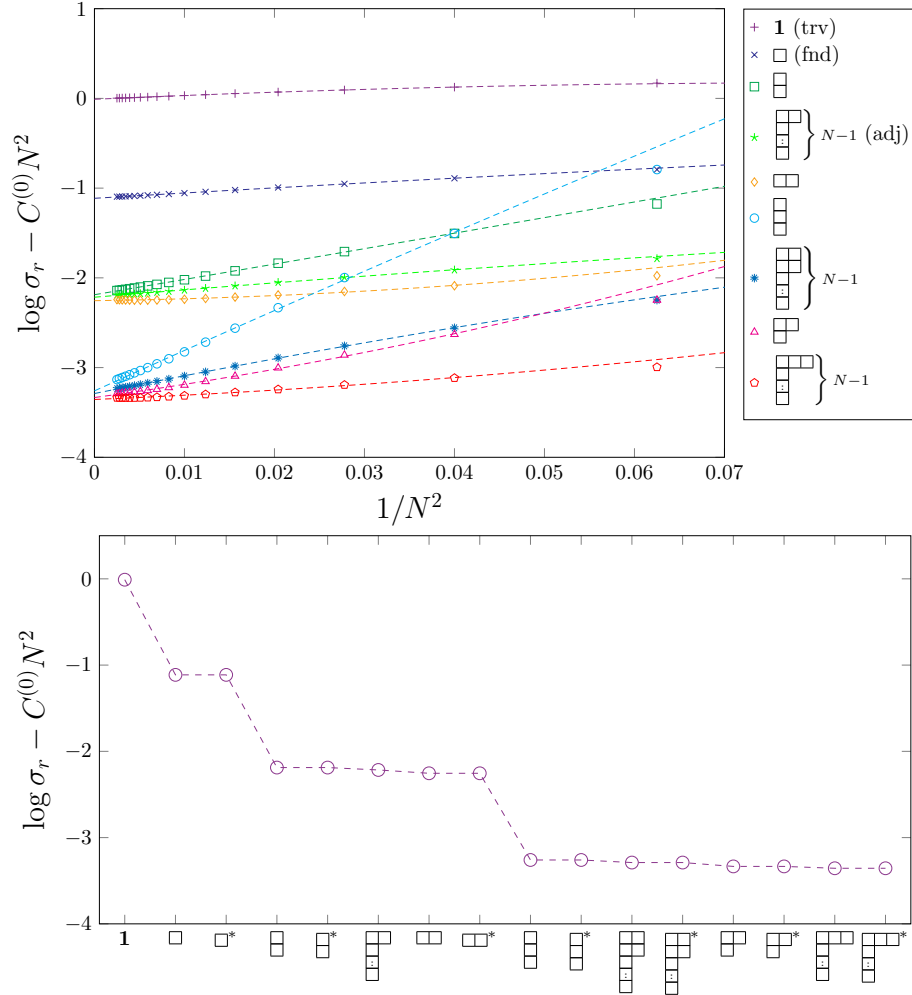


Figure 9: (Top) The quantity  $(\log \sigma_r - C^{(0)} N^2)$  is plotted against  $1/N^2$  for the  $SU(N)$  gauge theory with  $\lambda = 3$ . Different symbols correspond to different sequences of representations as shown on the right. Each point is actually doubly degenerate except for real representations since representations that are complex conjugate to each other give identical singular values. The dashed lines represent fits to a quadratic polynomial in  $1/N^2$  for each sequence using  $N \geq 5$ . (Bottom) The large- $N$  limit of  $(\log \sigma_r - C^{(0)} N^2)$  obtained from the top panel is shown for each sequence of representations in the descending order.

Let us start with the  $SU(N)$  gauge theories. We observe that the singular-value spectrum has a large- $N$  behavior consistent with

$$\log \sigma_r = \sum_{k=0}^{\infty} C_r^{(k)} N^{2(1-k)} = C_r^{(0)} N^2 + C_r^{(1)} + C_r^{(2)} N^{-2} + \dots, \quad (4.12)$$

where  $r$  corresponds to a sequence of representations for increasing  $N$  and  $C_r^{(k)}$  depend on the coupling constant  $\lambda$ . In Fig. 8 we plot  $\frac{1}{N^2} \log \sigma_r$  against  $\frac{1}{N^2}$  for the  $SU(N)$  gauge theory<sup>5</sup> with  $\lambda = 3$ . All the sequences listed here, which correspond to 16 largest singular values in the large- $N$  limit, can be fitted by (4.12) including terms up to  $k = 4$ . It is remarkable that the fit works nicely including the data points for  $N = 2$ . In fact, we find that the large- $N$  limit  $C_r^{(0)} = \lim_{N \rightarrow \infty} \frac{1}{N^2} \log \sigma_r$  for any sequence of representations is universal, and it is given by  $C^{(0)}$  defined in (4.6). Thus we conclude that the ratio of the singular values  $\sigma_r/\sigma_{\text{trv}}$  is finite in the large- $N$  limit. In other words, the singular-value spectrum has a definite profile given by  $C_r^{(1)}$  in the large- $N$  limit up to an overall factor.

We can obtain the large- $N$  limit of the singular-value spectrum explicitly as follows. In Fig. 9 (Top) we plot  $(\log \sigma_r - C^{(0)} N^2)$  against  $1/N^2$  for the  $SU(N)$  gauge theory with  $\lambda = 3$ . Fitting the data for  $N \geq 5$  to a quadratic polynomial for each sequence, we can make an extrapolation to  $N = \infty$ . In Fig. 9 (Bottom) we plot the large- $N$  limit of  $(\log \sigma_r - C^{(0)} N^2)$  thus obtained for each sequence of representations in the descending order.

Next let us consider the  $U(N)$  case. The large- $N$  behavior of the singular-value spectrum changes qualitatively as one crosses the critical point  $\lambda = 2$  of the Gross-Witten-Wadia phase transition (4.6). In Fig. 10, we plot the singular values  $\frac{1}{N^2} \log \sigma_r$  for the trivial (black circles), fundamental (black triangles) and adjoint representations (black squares) of  $U(N)$  against  $1/N^2$  in the  $U(N)$  gauge theory with  $\lambda = 1.5$  (Top) and  $\lambda = 3$  (Bottom). We also add some charge to these representations and plot the corresponding singular values in the same figure with different colors<sup>6</sup>. In both cases, the large- $N$  limit of  $\frac{1}{N^2} \log \sigma_r$  is common to all representations and agree with (4.6), but the way the limit is approached turns out to be qualitatively different for  $\lambda = 1.5$  and  $\lambda = 3$ .

---

<sup>5</sup>We have obtained qualitatively the same behavior at  $\lambda = 1.5$ , which is below the Gross-Witten-Wadia phase transition point  $\lambda = 2$ , in contrast to the situation in the  $U(N)$  case discussed below.

<sup>6</sup>Since the fundamental representation is not real unlike the trivial and adjoint representations, the representations one gets by adding charge  $\pm q$  to it are not complex conjugate to each other and hence the corresponding singular values acquires  $1/N$  terms with opposite signs as we see in Section 6.2. Here we take an average of the results for the representations with charge  $\pm q$  to cancel the  $1/N$  terms for the sake of simplicity.

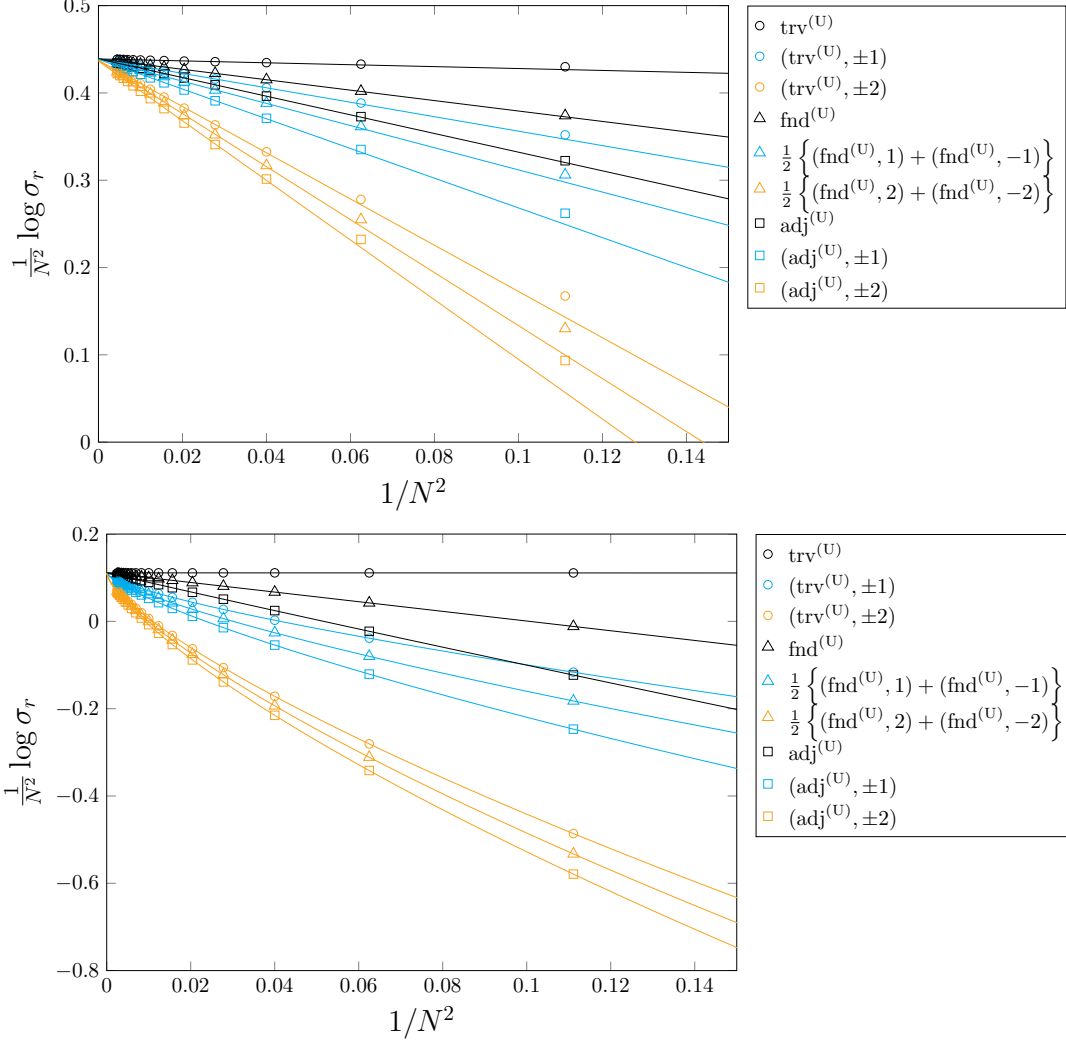


Figure 10: (Top) The singular values  $\frac{1}{N^2} \log \sigma_r$  for the trivial (black circles), fundamental (black triangles) and adjoint (black squares) representations of  $U(N)$  are plotted against  $1/N^2$  for the  $U(N)$  gauge theory with  $\lambda = 1.5$ . We also add some charge to these representations and plot the corresponding singular values in the same figure with different colors. The lines represent fits of the results for each representation with  $N \geq 7$  to  $C + c/N^2$  for  $\lambda = 1.5$ . (Bottom) A similar plot for  $\lambda = 3$ . The lines represent fits of the results for each representation with  $N \geq 3$  to  $C + a/N + b\chi_N/N^2 + c/N^2$ . The fits for the sequence of representations without charge yield  $a = b = 0$  within fitting errors.

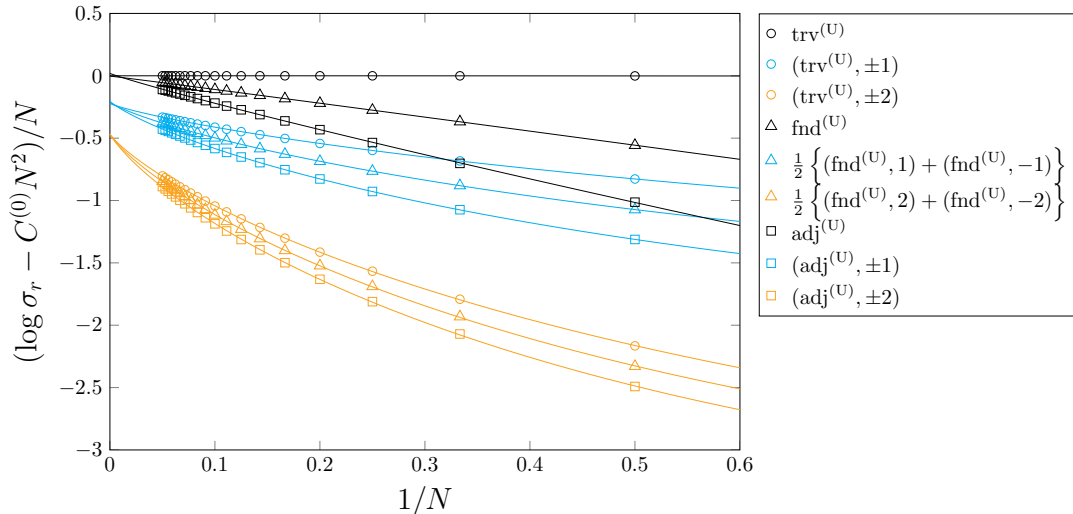


Figure 11: The quantity  $(\log \sigma_r - C^{(0)}N^2)/N$  is plotted against  $1/N$  for the trivial, fundamental and adjoint representations in the  $U(N)$  gauge theory with  $\lambda = 3$ . We also plot the same quantity for representations with nonzero charge with different colors. The lines represent fits of the results for each representation with  $N \geq 2$  to  $a + b\chi_N/N + c/N$ . For the sequences of representations without charge, the fits yield  $a = b = 0$  within fitting errors.

In the weak coupling phase  $\lambda < 2$ , we find that the singular values behave as<sup>7</sup>

$$\log \sigma_r = C^{(0)}N^2 + C_r^{(1)} + O\left(\frac{1}{N}\right). \quad (4.13)$$

The coefficient  $C^{(0)}$  of the leading term is common to all representations and is given by (4.6), while the coefficient  $C_r^{(1)}$  for the sub-leading term depends on the sequence of representations. This is confirmed in Fig. 10 (Top). Thus, the singular-value spectrum has a definite profile given by  $C_r^{(1)}$ , which is different from that in the  $SU(N)$  case.

In the strong coupling phase  $\lambda > 2$ , the large- $N$  behavior of the singular-value spectrum turns out to be more complicated. We find that the singular values behave as (4.13) for the sequence (4.10) of representations without charge. For sequences of representations (4.11) with nonzero charge, the singular values behave as

$$\log \sigma_r = C^{(0)}N^2 + C_r^{(1)} + aN + b\chi_N + O\left(\frac{1}{N}\right) \quad (4.14)$$

at large  $N$ , where the definition of  $\chi_N$  is given in (6.12), which has an  $O(\log N)$  term for  $\lambda > 2$  that we are considering. Note that (4.14) involves an  $O(N)$  term, whose coefficient  $a$  turns

<sup>7</sup>The  $1/N$  terms appear for the complex representations with nonzero charge.

out to be negative. This implies that the corresponding singular values are exponentially suppressed as  $\sigma_r/\sigma_{\text{trv}} \sim e^{-|a|N}$  at large  $N$ , and hence disappear from the singular-value spectrum in the large- $N$  limit. These behaviors are confirmed in Fig. 10 (Bottom).

The coefficient of the  $O(N)$  term is actually the same for the same charge, as can be seen from Fig. 11, where we plot  $(\log \sigma_r - C^{(0)}N^2)/N$  against  $1/N$ . We find that the curves merge at the same point at  $N = \infty$  for the same charge. A theoretical understanding of the  $O(N)$  term as well as the term involving  $\chi_N$  in (4.14) is provided in Section 6.2.

Note also that (2.11) implies

$$\sigma_{r^{(\text{SU})}} = \sum_{q=-\infty}^{\infty} \sigma_{(r^{(\text{U})}, q)} . \quad (4.15)$$

This has an interesting implication for  $\lambda > 2$  since in that case the sum on the right-hand side is dominated at large  $N$  by a single term with  $q = 0$ . Namely, the ratio of the singular value of  $(r^{(\text{U})}, 0)$  to that of the corresponding  $r^{(\text{SU})}$  becomes unity in the large- $N$  limit. This means that the coefficient  $C_r^{(1)}$  in (4.12) and (4.13) representing the sub-leading term is common to the  $U(N)$  and  $SU(N)$  gauge theories for the corresponding representations. Thus, for  $\lambda > 2$ , the singular-value spectrum for the  $U(N)$  gauge theory not only has a definite profile in the large- $N$  limit but also agrees with the profile for the  $SU(N)$  gauge theory.

#### 4.4 a novel interpretation of the Eguchi-Kawai reduction

In this section, we discuss the implications of the properties of the singular-value spectrum found in the previous section. In particular, we provide a new interpretation of the Eguchi-Kawai reduction [31], which states the volume independence in the large- $N$  limit.

As we have seen in the previous section, the leading large- $N$  behavior of the singular values  $\sigma_r$  is given by  $e^{C^{(0)}N^2}$  independently of the sequence of representations for both  $SU(N)$  and  $U(N)$  gauge theories, where  $C^{(0)}$  is given by (4.6). Factoring out this common factor, one obtains a finite large- $N$  limit

$$\lim_{N \rightarrow \infty} e^{-C^{(0)}N^2} \sigma_r = e^{C_r^{(1)}} , \quad (4.16)$$

which depends on the sequence of representations  $r$ . In the  $U(N)$  gauge theory at  $\lambda > 2$ , the limit in (4.16) becomes nonzero only for sequences of representations without charge, which agrees with the limit for the corresponding sequences of representations in the  $SU(N)$  gauge theory. Using (4.16) in (4.4), we find that the free energy density is given by

$$F \equiv \frac{1}{N^2V} \log Z = C^{(0)} + \frac{1}{VN^2} \log \left( \sum_r e^{VC_r^{(1)}} \right) + \dots , \quad (4.17)$$

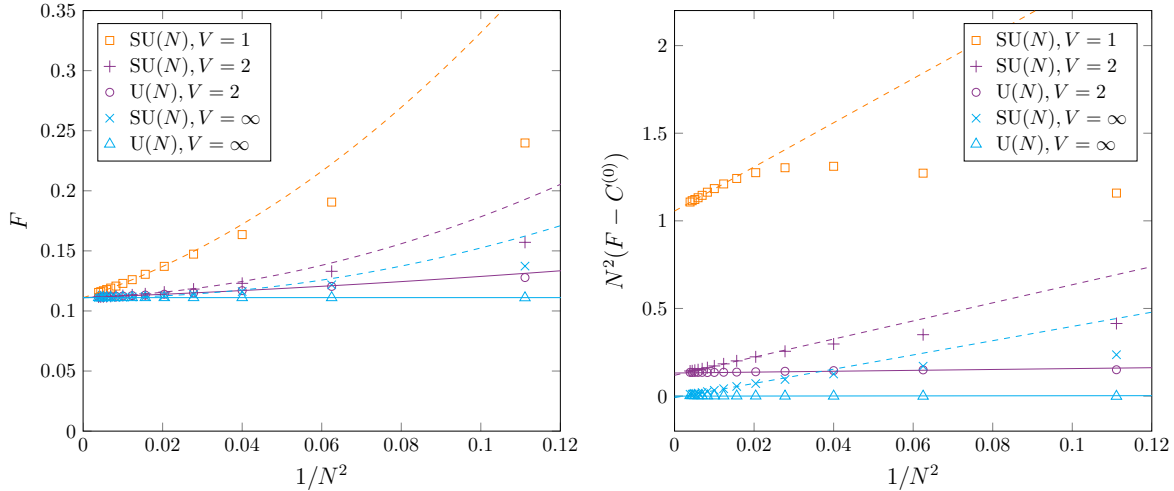


Figure 12: (Left) The free energy density  $F$  is plotted against  $1/N^2$  for the  $U(N)$  and  $SU(N)$  gauge theories at  $\lambda = 3$  with  $V = 1, 2$  and  $\infty$  using the bond dimension  $D_{\text{cut}} = 64$ . In the case of  $V = 1$ , there is no distinction between  $U(N)$  and  $SU(N)$  gauge theories, so we plot only the results for the latter. The solid and dashed lines are fits to the function  $a + b/N^2 + c/N^4$  for the  $U(N)$  and  $SU(N)$  gauge theories, respectively. (Right) The quantity  $N^2(F - C^{(0)})$  is plotted against  $1/N^2$  for the  $U(N)$  and  $SU(N)$  gauge theories at  $\lambda = 3$  with  $V = 1, 2$  and  $\infty$  using the bond dimension  $D_{\text{cut}} = 64$ . The solid and dashed lines are fits to the function  $a + b/N^2$  for the  $U(N)$  and  $SU(N)$  gauge theories, respectively. The extrapolated values at  $N = \infty$  give the coefficients of the  $O(1/N^2)$  terms in the free energy density  $F$ .

which implies that the free energy density becomes volume independent in the large- $N$  limit, and it is given by (4.6). This is nothing but the Eguchi-Kawai reduction [31].

In Fig. 12 (Left), we plot the free energy density  $F$  against  $1/N^2$  for the  $U(N)$  and  $SU(N)$  gauge theories at  $\lambda = 3$  with  $V = 1, 2$  and  $\infty$  using the bond dimension  $D_{\text{cut}} = 64$ , which is large enough as we see in Section 5.1. The results for  $V = \infty$  converge to (4.6) in the large- $N$  limit as it should<sup>8</sup>, but we also observe that the results for  $V = 1$  and  $2$  converge to the same value, which confirms the Eguchi-Kawai reduction.

In fact, we find that the results for  $V = 1$  are the same for the  $U(N)$  and  $SU(N)$  gauge theories even at finite  $N$  as one can see by setting  $V = 1$  in (4.4) and using (4.15). This can be understood from the fact that the two theories are equivalent at  $V = 1$  since the  $U(1)$

<sup>8</sup>In the case of  $U(N)$  gauge theory at  $V = \infty$ , we find that the free energy density is actually independent of  $N$ , which is due to the fact that the singular value for the trivial representation is given by  $\sigma_{\text{trv}} = C^{(0)}N^2$  for arbitrary  $N$  in the strong coupling phase  $\lambda > 2$  as one can see from Fig. 10 (Bottom).

part of the gauge field cancels in the plaquette (2.4). We also notice from our argument above that at  $\lambda > 2$ , the  $O(1/N^2)$  term in (4.17) should agree for the  $U(N)$  and  $SU(N)$  gauge theories. This is confirmed in Fig. 12 (Right) for  $V = 2$  by extrapolating  $N^2(F - C^{(0)})$  to  $N = \infty$ , which gives identical values for the  $U(N)$  and  $SU(N)$  gauge theories. Note that this statement does not hold at  $\lambda < 2$ .

Thus, the Eguchi-Kawai reduction in the present model results from the simple  $V$ -dependence of the partition function (4.4) and the large- $N$  behavior (4.16) of the singular values with the common  $C^{(0)}$ . The simple  $V$ -dependence (4.4) may also be viewed as a consequence of the fact that the singular-value spectrum of the fundamental tensor has certain self-similarity under the coarse-graining procedure as seen in (4.2) and (4.3).

In  $d \geq 3$  dimensional cases, the volume independence in the  $N \rightarrow \infty$  limit is expected only for  $V > V_{\text{cr}}$  since the SSB of  $U(1)^d$  symmetry [37] occurs for  $V \leq V_{\text{cr}}$  [38, 39], which invalidates the proof of the Eguchi-Kawai reduction [31]. Note also that the partition function does not take a simple form like (4.4) any more. However, we speculate that the volume independence for  $V > V_{\text{cr}}$  may be understood by some sort of self-similarity that manifests itself after some steps of coarse graining at large  $N$ .

## 5 Explicit results with a bond dimension $D_{\text{cut}}$

Given the singular values of the fundamental tensor up to some bond dimension  $D_{\text{cut}}$ , we can obtain explicit results for various observables. We discuss how the results depend on  $D_{\text{cut}}$ , and show, in particular, that the finite  $D_{\text{cut}}$  effects become severe for small  $N$ , small volume and at weak coupling. We can obtain explicit results even in such cases. As an example, we show how the Gross-Witten-Wadia phase transition appears as  $N$  increases.

### 5.1 the $D_{\text{cut}}$ -dependence

Let us first discuss the  $D_{\text{cut}}$ -dependence. Since the observables are typically obtained by taking the derivatives of the free energy density  $F$  (4.17) in the TRG, let us consider the  $D_{\text{cut}}$ -dependence of  $F$ . Note first that the  $D_{\text{cut}}$ -dependence disappears in the infinite-volume limit since the trivial representation dominates in that limit as we mentioned at the end of Section 4.1. Therefore, we focus on the free energy density  $\tilde{F}(D_{\text{cut}})$  obtained for finite  $D_{\text{cut}}$  with  $V = 1$ , where finite  $D_{\text{cut}}$  effects become the severest.

In Fig. 13 (Left), we plot the free energy density  $\left\{ \tilde{F}(D_{\text{cut}}) - \tilde{F}(1) \right\}$  against  $D_{\text{cut}}$  for the  $SU(3)$  gauge theory with various values of the coupling constant, which are used also in Fig. 7. We find that the free energy density converges faster at stronger coupling. This

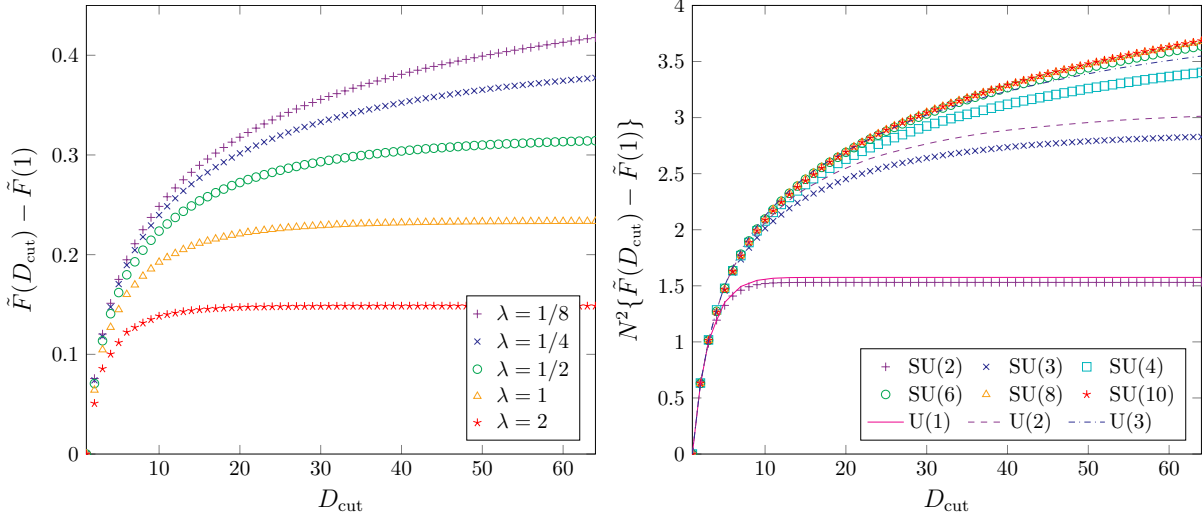


Figure 13: (Left) The free energy density  $\{\tilde{F}(D_{\text{cut}}) - \tilde{F}(1)\}$  for  $V = 1$  is plotted against  $D_{\text{cut}}$  for the SU(3) gauge theory with various values of the coupling constant, which are used also in Fig. 7. (Right) The free energy density  $N^2\{\tilde{F}(D_{\text{cut}}) - \tilde{F}(1)\}$  for  $V = 1$  is plotted with different normalization against  $D_{\text{cut}}$  for the U( $N$ ) and SU( $N$ ) gauge theories with various  $N$  at  $\lambda = 0.5$ .

is consistent with the singular-value distribution in Fig. 7, which falls off faster at larger  $\lambda$ .

In fact, the finite  $D_{\text{cut}}$  effects vanish as  $O(1/N^2)$  at large  $N$  since finite volume effects, which cause the finite  $D_{\text{cut}}$  effects, are suppressed by  $1/N^2$  due to the Eguchi-Kawai reduction. In order to see this more explicitly, let us note that the free energy density  $\tilde{F}(D_{\text{cut}})$  at finite  $D_{\text{cut}}$  and  $V = 1$  has the large- $N$  behavior

$$\tilde{F}(D_{\text{cut}}) = C^{(0)} + \frac{1}{N^2}f(D_{\text{cut}}) + \cdots, \quad (5.1)$$

$$f(D_{\text{cut}}) \equiv \log \sum_{i=1}^{D_{\text{cut}}} \exp(C_{r_i}^{(1)}), \quad (5.2)$$

as one can see from (4.17). In Fig. 13 (Right) we plot  $N^2\{\tilde{F}(D_{\text{cut}}) - \tilde{F}(1)\}$  against  $D_{\text{cut}}$ , where the results are seen to approach a single curve in the large- $N$  limit<sup>9</sup>, which corresponds to the function  $f(D_{\text{cut}})$  that appears in (5.1). Note that the equivalence between the U( $N$ ) and SU( $N$ ) gauge theories at  $V = 1$  holds in the  $D_{\text{cut}} \rightarrow \infty$  limit but not for finite  $D_{\text{cut}}$ . In fact, the finite  $D_{\text{cut}}$  effects are smaller for SU( $N$ ) with the same  $N$ , as one can see from Fig. 13 (Right), since the sum over the charge is taken already in (2.11).

<sup>9</sup>This curve is not common to the U( $N$ ) and SU( $N$ ) gauge theories for  $\lambda = 0.5$  used here. However, it is common for  $\lambda > 2$  due to the agreement of the coefficients  $C_r^{(1)}$  in the two theories.



## 5.2 Gross-Witten-Wadia phase transition

As a demonstration of how the TRG works, let us discuss the Gross-Witten-Wadia phase transition (4.6), which occurs in the large- $N$  limit. By taking the derivative of the free energy density (4.17), we define the average plaquette and the specific heat as

$$W = -\frac{\lambda^2}{2} \frac{\partial F}{\partial \lambda}, \quad C = -2 \frac{\partial W}{\partial \lambda}, \quad (5.3)$$

whose large- $N$  limits are given by [28, 29]

$$\lim_{N \rightarrow \infty} W = \begin{cases} 1 - \frac{\lambda}{4} & (\lambda < 2), \\ \frac{1}{\lambda} & (\lambda \geq 2), \end{cases} \quad \lim_{N \rightarrow \infty} C = \begin{cases} \frac{1}{2} & (\lambda < 2), \\ \frac{2}{\lambda^2} & (\lambda \geq 2). \end{cases} \quad (5.4)$$

In order to calculate observables, we take the derivatives of the partition function numerically using the 9-point central finite difference schemes [40]

$$\begin{aligned} \epsilon f'(x) &= \frac{4}{5}f(x + \epsilon) - \frac{1}{5}f(x + 2\epsilon) + \frac{4}{105}f(x + 3\epsilon) - \frac{1}{280}f(x + 4\epsilon) \\ &\quad - \frac{4}{5}f(x - \epsilon) + \frac{1}{5}f(x - 2\epsilon) - \frac{4}{105}f(x - 3\epsilon) + \frac{1}{280}f(x - 4\epsilon), \end{aligned} \quad (5.5)$$

$$\begin{aligned} \epsilon^2 f''(x) &= -\frac{205}{72}f(x) + \frac{8}{5}f(x + \epsilon) - \frac{1}{5}f(x + 2\epsilon) + \frac{8}{315}f(x + 3\epsilon) - \frac{1}{560}f(x + 4\epsilon) \\ &\quad + \frac{8}{5}f(x - \epsilon) - \frac{1}{5}f(x - 2\epsilon) + \frac{8}{315}f(x - 3\epsilon) - \frac{1}{560}f(x - 4\epsilon) \end{aligned} \quad (5.6)$$

with  $\epsilon = 0.01$ .

In Fig. 14, we plot the specific heat obtained by differentiating the free energy density numerically for the SU(3) (Left) and SU(10) (Right) gauge theories with various  $L$ . The bond dimension is chosen to be  $D_{\text{cut}} = 64$ . We see that the finite volume effects are reduced considerably by increasing  $N$  from 3 to 10 due to the Eguchi-Kawai reduction. We also see how the Gross-Witten-Wadia phase transition appears as  $N$  increases.

## 6 2D $U(N)$ gauge theory with the $\theta$ term

In this section, we show how the TRG works when we add a  $\theta$  term to the 2D gauge theory. Exact solutions are obtained and discussed in Refs. [41, 42]. This model is of particular interest since ordinary Monte Carlo simulation becomes extremely difficult due to the sign problem. Recently the complex Langevin method [43] and the density-of-state method [44] were applied to this model successfully. (See also Ref. [45].) In these studies, however, one has to dismiss periodic boundary conditions in order to avoid the topology freezing problem, which refers to the problem that one cannot sample configurations in different topological

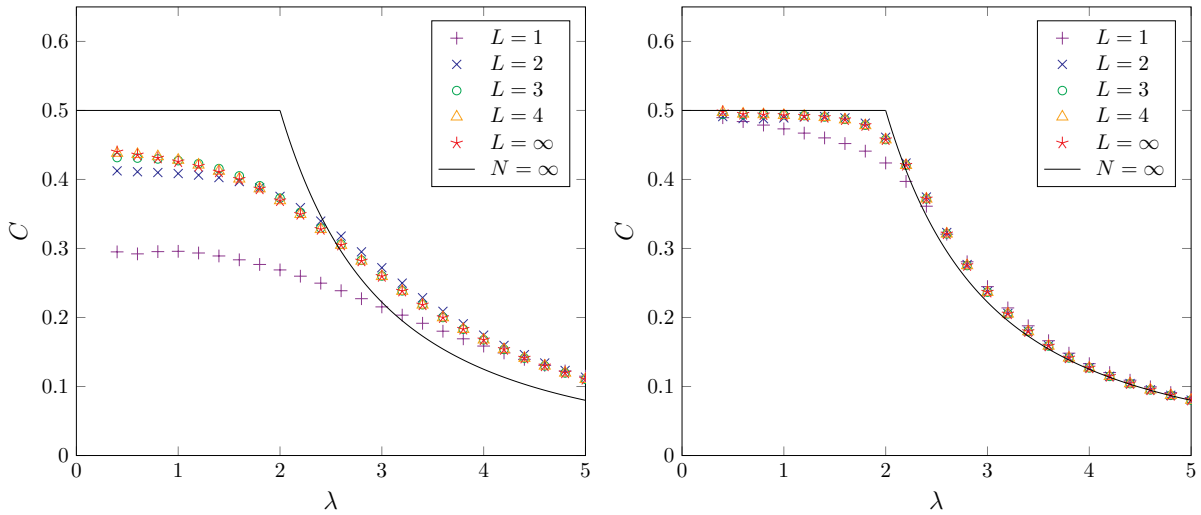


Figure 14: The specific heat  $C$  defined in (5.3) is plotted against the 't Hooft coupling constant  $\lambda$  for the SU(3) (Left) and SU(10) (Right) gauge theories with various  $L$  using  $D_{\text{cut}} = 64$ . The solid line represents the large- $N$  limit obtained analytically as (5.4).

sectors with the correct weight. The TRG is not only free from the sign problem but also free from the topology freezing problem. It therefore allows us to obtain results even with periodic boundary conditions unlike in Refs. [43, 44]. In the U(1) case, the TRG was applied to this model using the Gauss quadrature instead of the character expansion in order to discretize the indices of the fundamental tensor [24].

## 6.1 the first-order phase transition at $\theta = \pm\pi$

In two dimensions, the  $\theta$  term in the continuum action reads

$$S_\theta = -i\theta Q, \quad (6.1)$$

$$Q = \frac{1}{4\pi} \int d^2x \epsilon_{\mu\nu} \text{tr} F_{\mu\nu}, \quad (6.2)$$

where the topological charge  $Q$  takes integer values on a compact manifold. Since the topological charge  $Q$  vanishes identically for the SU( $N$ ) case in 2D, we restrict ourselves to the U( $N$ ) case in this section. Putting the theory on a periodic lattice, the action is given by the plaquette action (2.3) with an additional term (6.1), where the definition of the topological charge  $Q$  is given on the lattice by

$$Q = \frac{1}{2\pi i} \sum_n \log \det P_n. \quad (6.3)$$

The complex log in (6.3) is defined by using the principal value. The topological charge  $Q$  thus defined takes integer values even before taking the continuum limit, which guarantees that the partition function is invariant under  $\theta \mapsto \theta + 2\pi$ .

The exact solution for the theory with the  $\theta$  term can be obtained as in the  $\theta = 0$  case discussed in Section 2. Corresponding to (2.29), one obtains [41]

$$Z(\theta) = \sum_r \left( \frac{\tilde{\gamma}_r(\theta)}{d_r} \right)^{L_1 L_2}, \quad (6.4)$$

$$\tilde{\gamma}_r(\theta) = \det \mathcal{M}_r(\theta), \quad (6.5)$$

$$[\mathcal{M}_r(\theta)]_{ij} = \int_{-\pi}^{+\pi} \frac{d\phi}{2\pi} \cos\{(l_j + i - j + \frac{\theta}{2\pi})\phi\} \exp\left(\frac{2N}{\lambda} \cos \phi\right), \quad (6.6)$$

and corresponding to (4.1), the singular values become

$$\sigma_r(\theta) = \frac{|\tilde{\gamma}_r(\theta)|}{d_r}. \quad (6.7)$$

Note that (6.6) implies that the singular values have the properties

$$\sigma_{(r^{(U)}, q)}(\theta + 2\pi) = \sigma_{(r^{(U)}, q+1)}(\theta), \quad (6.8)$$

$$\sigma_{r^{(U)}}(-\theta) = \sigma_{\bar{r}^{(U)}}(\theta). \quad (6.9)$$

Namely the singular values are not invariant under  $\theta \mapsto \theta + 2\pi$  or  $\theta \mapsto -\theta$ , while the partition function is, because of the summation over representations  $r$  involved in (6.4).

The most interesting feature of this theory is the existence of the first-order phase transition at  $\theta = \pi$ , which is associated with the spontaneous breaking of the parity symmetry. In order to see this, let us first note that the expectation value of the topological charge  $Q$  is pure imaginary for arbitrary  $\theta$  due to the fact that  $Q$  is real and parity odd. We therefore define the topological charge density as

$$\frac{1}{V} \text{Im}\langle Q \rangle = -\frac{1}{V} \frac{\partial}{\partial \theta} \log Z(\theta), \quad (6.10)$$

which develops a gap at  $\theta = \pm(\pi - \epsilon)$  for  $\epsilon \rightarrow +0$  as the volume  $V$  increases. In Fig. 15 we plot the topological charge density<sup>10</sup> against  $\theta$  for the U(3) gauge theory with various  $L$  using  $D_{\text{cut}} = 32$  and  $\lambda = 3$ , which exhibits a clear gap at  $\theta = \pm\pi$  with increasing  $L$ .

From now on, we discuss the large- $N$  behavior of the theory with the  $\theta$  term. Let us first mention that the topological susceptibility defined by

$$\chi = -\lim_{V \rightarrow \infty} \frac{1}{V} \frac{\partial^2}{\partial \theta^2} \log Z(\theta) \Big|_{\theta=0} = \lim_{V \rightarrow \infty} \frac{1}{V} \left( \langle Q^2 \rangle - \langle Q \rangle^2 \right) \Big|_{\theta=0} \quad (6.11)$$

---

<sup>10</sup>We find that the topological charge vanishes identically for  $L = 1$ . This is expected from the fact that the one-site model cannot distinguish U( $N$ ) and SU( $N$ ) as we explained in Section 4.4.

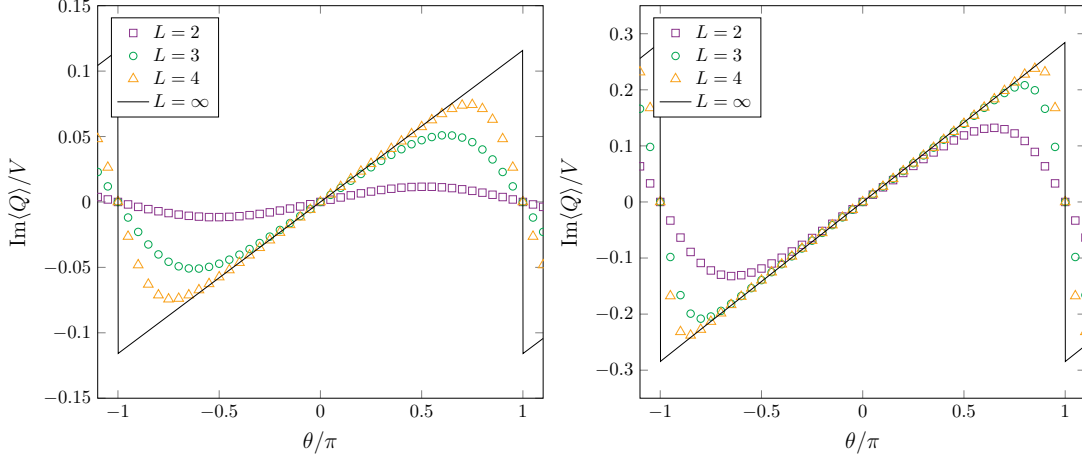


Figure 15: The imaginary part of the topological charge density is plotted against  $\theta$  for the  $U(3)$  gauge theory with various  $L$ ,  $D_{\text{cut}} = 32$  using  $\lambda = 1.5$  (Left) and  $\lambda = 3$  (Right). A clear gap is seen to develop at  $\theta = \pm\pi$  with increasing  $L$ .

is obtained at large  $N$  as [41]

$$\chi \sim \chi_N \equiv \begin{cases} -\frac{1}{4\pi^2} \log\left(1 - \frac{\lambda}{2}\right) & \text{for } \lambda < 2, \\ \frac{1}{2\pi^2} \left\{ \log N + \log\left(1 - \frac{2}{\lambda}\right) + \gamma_E + 1 \right\} & \text{for } \lambda > 2, \end{cases} \quad (6.12)$$

where  $\gamma_E \approx 0.5772$  is the Euler constant. Notice the appearance of  $\log N$  for  $\lambda > 2$ . Since  $\text{Im}\langle Q\rangle/V \sim \chi_N \theta$  at small  $\theta$ , we consider the quantity  $\text{Im}\langle Q\rangle/(V\chi_N)$ , which is normalized by  $\chi_N$ , in order to make the quantity finite in the  $N \rightarrow \infty$  limit.

In Fig. 16, we plot  $\text{Im}\langle Q\rangle/(V\chi_N)$  against  $\theta$  in the  $U(N)$  gauge theory for various  $N$  with  $L = 2$ ,  $D_{\text{cut}} = 32$  using  $\lambda = 1.5$  (Left) and  $\lambda = 3$  (Right). We find that the results for  $\lambda = 3$  approach the results for  $L = \infty$  as  $N$  increases, whereas the results for  $\lambda = 1.5$  do not<sup>11</sup>. This suggests that the volume independence holds in the large- $N$  limit in the strong coupling phase. In fact, we see in Fig. 15 that finite volume effects are considerably reduced for  $\lambda = 3$  compared with  $\lambda = 1.5$ , which shows some tendencies towards the volume independence for  $\lambda > 2$  already at  $N = 3$ . We will provide a theoretical understanding of this novel volume independence based on the large- $N$  behavior of the singular-value spectrum in the presence of the  $\theta$  term.

<sup>11</sup>We also find in Fig. 16 that the results for  $\lambda = 1.5$  become completely linear in  $\theta$  in the  $L \rightarrow \infty$  and  $N \rightarrow \infty$  limits, whereas the results for  $\lambda = 3$  do not. This can be understood from the large- $N$  behavior of the singular values given by (6.14) and (6.17) for  $\lambda < 2$  and  $\lambda > 2$ , respectively.

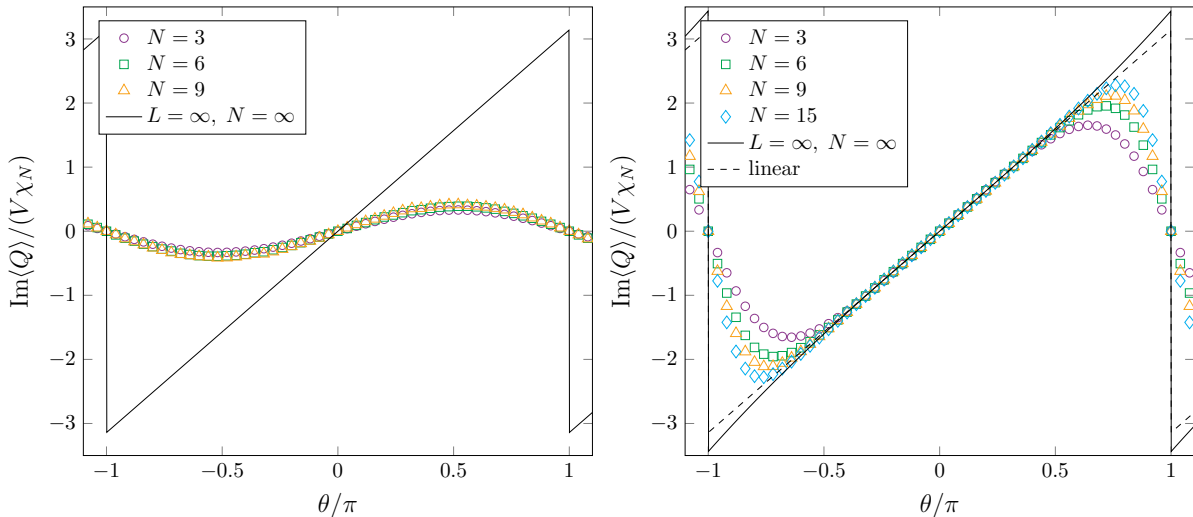


Figure 16: The imaginary part of the topological charge density is plotted against  $\theta$  for  $U(N)$  gauge theories with various  $N$  and  $L = 2$ ,  $D_{\text{cut}} = 32$  using  $\lambda = 1.5$  (Left) and  $\lambda = 3$  (Right). The results for  $N = \infty$  and  $L = \infty$  are shown by the solid lines, which, for  $\lambda = 3$ , deviates from the linear behavior represented by the dashed line in the right panel.

## 6.2 the large- $N$ behavior of the singular-value spectrum

Let us recall here that the summation over representations in (6.4) is dominated by the trivial representation in the  $V \rightarrow \infty$  limit for any  $\theta$  in  $|\theta| < \pi$ . Therefore, (6.12) implies

$$\log \sigma_{\text{triv}(U)}(\theta) \sim \log \sigma_{\text{triv}(U)}(0) - \frac{1}{2} \chi_N \theta^2 \quad (6.13)$$

at  $\theta \sim 0$ . Note that  $\sigma_r(\theta)$  is an even function of  $\theta$  for real representations  $r$  in general due to the property (6.9). In what follows, we investigate the large- $N$  properties of the singular values for general representations.

Let us first discuss the weak coupling phase  $\lambda < 2$ . For the sequence (4.10) of representations without charge, we find that<sup>12</sup>

$$\log \sigma_{r(U)}(\theta) = \log \sigma_{r(U)}(0) - \frac{1}{2} \chi_N \theta^2 + \mathcal{O}\left(\frac{1}{N}\right) \quad (6.14)$$

at large  $N$ , where  $\chi_N$  is an  $\mathcal{O}(1)$  quantity given by (6.12). Note that the singular values  $\sigma_r(\theta)$  are not periodic in  $\theta$  as we mentioned below (6.8), and (6.14) holds for arbitrary  $\theta$ . This is shown in Fig. 17 (Top-Left) for the trivial, fundamental<sup>13</sup> and adjoint representations. The small deviation at large  $\theta$  is due to finite  $N$  effects as we can see from Fig. 17 (Bottom-Left).

<sup>12</sup>A linear term in  $\theta$  appears at  $\mathcal{O}(1/N)$  for complex representations but not for the real ones.

<sup>13</sup>Since the fundamental representation is not real unlike the trivial and adjoint representations, the  $1/N$

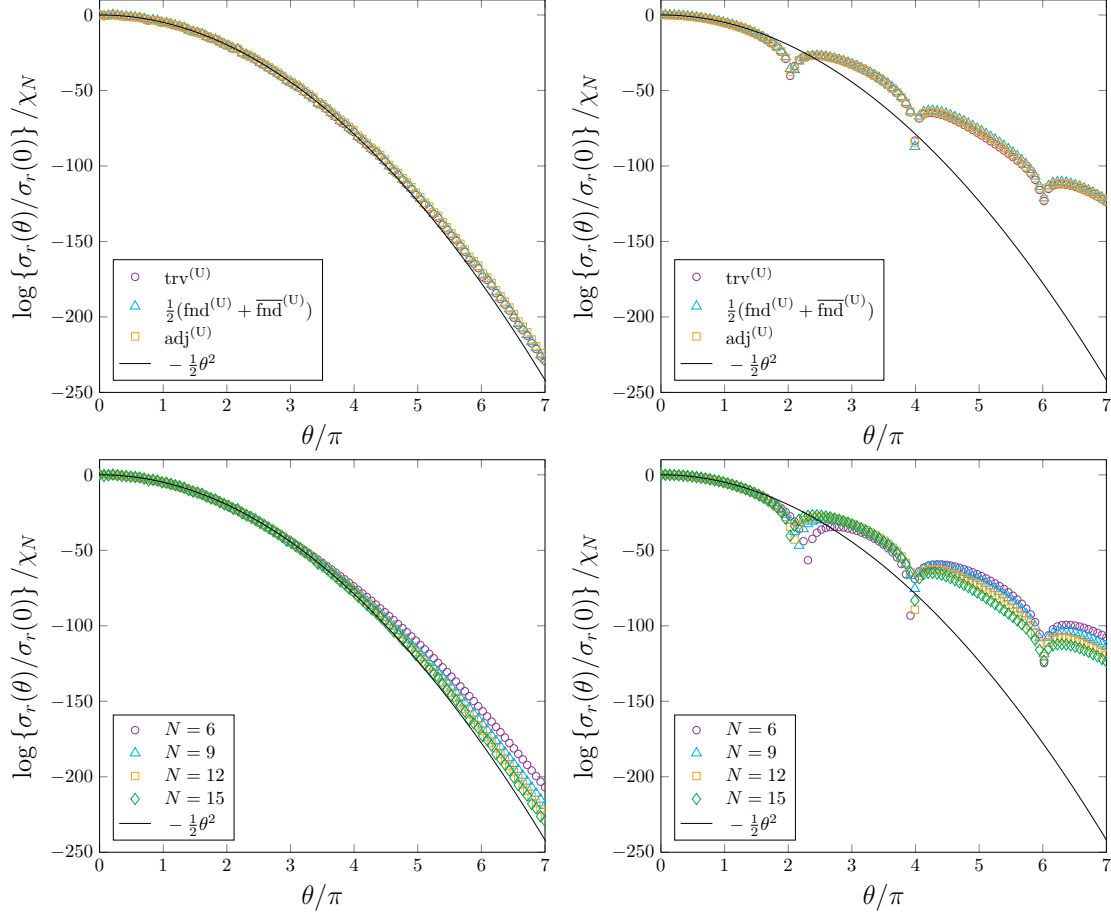


Figure 17: (Top) The quantity  $\frac{1}{\chi^N} \log\{\sigma_r(\theta)/\sigma_r(0)\}$  is plotted against  $\theta$  for the trivial, fundamental and adjoint representations in the  $U(N)$  gauge theory with  $N = 15$  at  $\lambda = 1.5$  (Left) and  $\lambda = 3$  (Right). We also show the behavior  $-\frac{1}{2}\theta^2$  by the solid lines for comparison. (Bottom) The same plots with various  $N$  at  $\lambda = 1.5$  (Left) and  $\lambda = 3$  (Right) are shown for the trivial representation. A clear large- $N$  scaling behavior is seen. Similar behaviors are observed for the other representations.

When we add some charge  $q$  to the representation  $r^{(U)}$ , we obtain

$$\sigma_{(r^{(U)}, q)}(\theta) = \sigma_{r^{(U)}}(\theta + 2\pi q) = \sigma_{r^{(U)}}(0) e^{-\frac{1}{2}\chi_N(\theta+2\pi q)^2 + O(1/N)} \quad (6.15)$$

using (6.8) and (6.14). Setting  $\theta = 0$  in (6.15), we get

$$\sigma_{(r^{(U)}, q)}(0) = \sigma_{r^{(U)}}(0) e^{-2\pi^2 q^2 \chi_N + O(1/N)}, \quad (6.16)$$

which provides a clear understanding of the results in Fig. 10 (Top), where  $\log \sigma_r$  for representations with some charge  $q$  has a slope commonly decreased by  $2\pi^2 q^2 \chi_N$ . When we switch on  $\theta$ , (6.15) implies that the singular-value spectrum still has a definite profile in the large- $N$  limit, and the  $\theta$ -dependence of the profile comes only from the factor  $e^{-\frac{1}{2}\chi_N(\theta+2\pi q)^2}$ , which depends on the charge  $q$ .

Let us next discuss the strong coupling phase  $\lambda > 2$ , where  $\chi_N$  involves a  $\log N$  term as in (6.12). For the sequence (4.10) of representations without charge, we observe from Fig. 17 (Top-Right) that

$$\log \sigma_{r^{(U)}}(\theta) = \log \sigma_{r^{(U)}}(0) - \chi_N \varphi(\theta) + O\left(\frac{1}{N}\right) \quad (6.17)$$

at large  $N$  except for  $\theta \sim 2n\pi$  ( $|n| = 1, 2, \dots$ ). The function  $\varphi(\theta)$  in (6.17) is given by some even function of  $\theta$ , which is independent of  $r^{(U)}$  and satisfy  $\varphi(\theta) \sim \frac{1}{2}\theta^2$  at small  $\theta$ .

At  $\theta \sim 2n\pi$  ( $|n| = 1, 2, \dots$ ), the function  $\varphi(\theta)$  has singularities, which appear because  $\tilde{\gamma}_{r^{(U)}}(\theta)$  in (6.7) oscillates around zero as a function of  $\theta$ . In the vicinity of these zeroes, which we denote by  $\theta_n(N)$ , we find that

$$\sigma_{r^{(U)}}(\theta) \sim \sigma_{r^{(U)}}(0) e^{b_n \chi_N + v_n} |\theta - \theta_n(N)|, \quad (6.18)$$

$$|\theta_n(N) - 2\pi n| \sim e^{a_n N + u_n} \quad (a_n < 0) \quad (6.19)$$

at large  $N$ . In Fig. 18, we confirm this behavior at  $\lambda = 3$  for the trivial representation, but the same scaling behavior is confirmed also for the fundamental and adjoint representations. In the top panel, we plot  $\tilde{\gamma}_{\text{trv}}(\theta)/\tilde{\gamma}_{\text{trv}}(0)$  against  $\theta$ , which shows that the ratio crosses zero at  $\theta = \theta_n(N) \sim 2\pi n$  for  $n = 1$ . In the bottom-left panel, we plot  $|\theta_n(N) - 2\pi n|$  against  $N$  in the log scale, which confirms (6.19) for  $n = 1, 2$  and  $3$ . In the bottom-right panel, we define the function  $K_n(\theta)$  by

$$\sigma_{r^{(U)}}(\theta) = \sigma_{r^{(U)}}(0) e^{K_n(\theta)} |\theta - \theta_n(N)| \quad (6.20)$$

---

terms in (6.14) involves a linear term in  $\theta$ . Here we take an average of the results for the fundamental and anti-fundamental representations to cancel this term for the sake of simplicity. This remark also applies to Fig. 19, where we add charge  $-1$  to the fundamental representation.

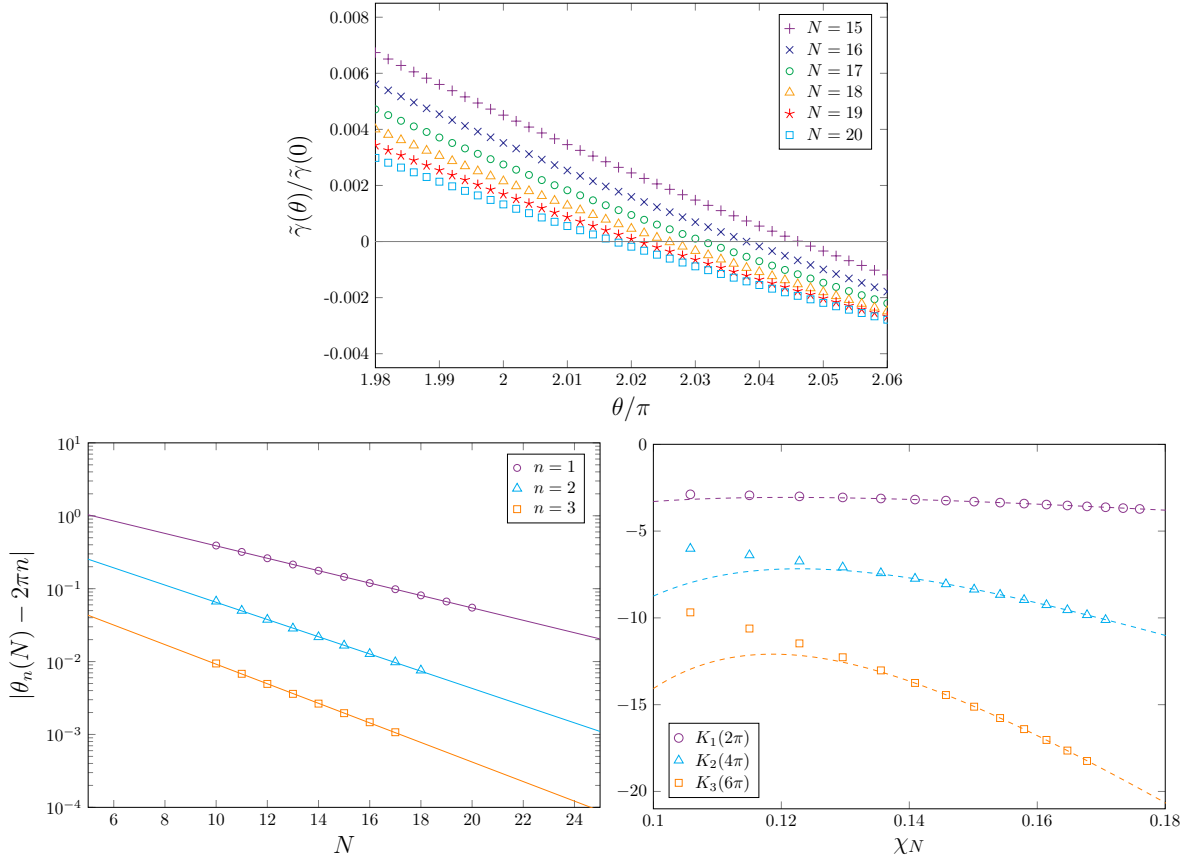


Figure 18: (Top) The ratio  $\tilde{\gamma}_{\text{trv}}(\theta)/\tilde{\gamma}_{\text{trv}}(0)$  for the trivial representation is plotted against  $\theta$  in the U(N) gauge theory with various N at  $\lambda = 3$ . (Bottom-Left) The deviation of the zeroes  $\theta_n(N)$  from  $2\pi n$  is plotted against N for  $n = 1, 2$  and 3 in the log scale. The solid lines are fits to the exponential behavior  $|\theta_n(N) - 2\pi n| \sim A_n e^{-B_n N}$ . (Bottom-Right) The quantity  $K_n(2\pi n)$  is plotted for  $n = 1, 2$  and 3 against  $\chi_N$ . The dashed lines are fits to the behavior  $K_n(2\pi n) = b_n \chi_N + c_n + d_n/N^2$ .



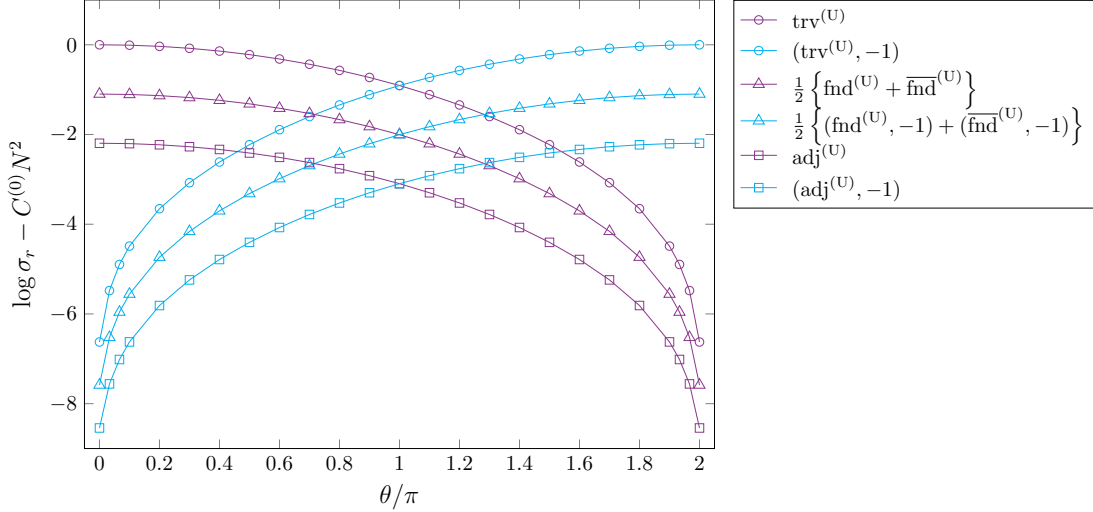


Figure 19: The quantity  $(\log(\sigma_r) - C^{(0)}N^2)$  is plotted against  $\theta$  for trivial, fundamental and adjoint representations in the  $U(N)$  gauge theory with  $N = 20$  at  $\lambda = 3$ . We also plot the results for representations with charge  $q = -1$  with blue symbols.

around  $\theta \sim \theta_n(N)$  and plot  $K_n(2\pi n)$  against  $\chi_N$  for  $n = 1, 2$  and  $3$ , which confirms (6.18) at large  $N$ .

Adding some charge  $q \neq 0$  to the representation  $r^{(U)}$  and setting  $\theta = 0$ , we obtain

$$\sigma_{(r^{(U)}, q)}(0) = \sigma_{r^{(U)}}(2\pi q) = \sigma_{r^{(U)}}(0) e^{a_q N + b_q \chi_N + c_q} , \quad (6.21)$$

using (6.8), (6.18) and (6.19), where we have defined  $c_n = u_n + v_n$ . This implies

$$\log \sigma_{(r^{(U)}, q)}(0) = \log \sigma_{r^{(U)}}(0) + a_q N + b_q \chi_N + c_q , \quad (6.22)$$

which provides a clear understanding of our results in Fig. 11. As we discussed in Section 4.3, the representations with some charge have a negative  $O(N)$  term with the same coefficient for the same charge and they all disappear from the spectrum at large  $N$ .

Let us discuss what happens for  $\theta \neq 0$ . Using (6.8) and (6.17), we obtain

$$\sigma_{(r^{(U)}, q)}(\theta) = \sigma_{r^{(U)}}(0) e^{-\chi_N \varphi(\theta + 2\pi q) + O(1/N)} . \quad (6.23)$$

This is confirmed in Fig. 19, where we plot  $(\log \sigma_r - C^{(0)}N^2)$  against  $\theta$  for various representations in the  $U(N)$  gauge theory with  $N = 20$  at  $\lambda = 3$ . We can see that the curves have the same  $\theta$  dependence for the same charge  $q$  neglecting the  $O(1/N)$  terms in (6.23). Note also that the representations with charge  $q = -1$  take over at  $\theta > \pi$ , which ensures the  $2\pi$  periodicity of the partition function.

Eq. (6.23) implies that it is also true for nonzero  $|\theta| < \pi$  that only the sequences (4.10) of representations without charge dominate in the large- $N$  limit at  $\lambda > 2$  since the coefficient of the negative  $O(\log N)$  term in  $\log \sigma_r$  is larger in magnitude for  $q \neq 0$ . Moreover, since the  $\theta$ -dependence comes only from the common overall factor  $e^{-\chi_N \varphi(\theta)}$  for the  $q = 0$  sector that dominates in the large- $N$  limit, the singular-value spectrum has a definite profile in the large- $N$  limit, which is  $\theta$ -independent. Let us recall that the profile at  $\theta = 0$  is the same as that for  $SU(N)$  in the  $\lambda > 2$  region as we discussed in Section 4.3. This profile remains unaltered at nonzero  $\theta$  up to the  $\theta$ -dependent overall factor<sup>14</sup>.

As an interesting consequence of this fact, we obtain the free energy corresponding to (4.17) as

$$\frac{1}{V} \log Z = C^{(0)} N^2 - \chi_N \varphi(\theta) + \frac{1}{V} \log \left( \sum_r e^{V C_r^{(1)}} \right) + \dots, \quad (6.24)$$

where the ellipsis represents the terms that vanish in the large- $N$  limit. Thus we find

$$\frac{1}{V} \text{Im} \langle Q \rangle = -\frac{1}{V} \frac{d}{d\theta} \log Z(\theta) = \chi_N \frac{d\varphi(\theta)}{d\theta} + \dots, \quad (6.25)$$

which is independent of  $V$  at large  $N$ . This explains our observation in Fig. 16. Note that the volume independence we find here goes beyond the Eguchi-Kawai reduction in that it refers to the  $O(1)$  terms in (6.24) instead of the  $O(N^2)$  term. It should be noted here that the leading  $O(N^2)$  term in the free energy cannot depend on  $\theta$  since the  $\theta$  term is sub-dominant to the kinetic term of the gauge field in the action at large  $N$ .

Let us also emphasize that (6.24) does not hold in the weak coupling phase  $\lambda < 2$  since the representations with all the charge  $q$  survive in that case, and they have a factor  $e^{-\frac{1}{2}\chi_N(\theta+2\pi q)^2}$ , which depends on  $q$ . Hence, this volume independence holds only for  $\lambda > 2$ .

## 7 Summary

In this paper, we discussed how the TRG can be applied to  $SU(N)$  and  $U(N)$  gauge theories by considering the 2D case, which is exactly solvable. Using the character expansion, the fundamental tensor turns out to be extremely simple as in (2.28), which results in a simple evolution of the singular-value spectrum with coarse graining. However, in actual calculation, we have to restrict the number of representations in the character expansion in

---

<sup>14</sup>In the  $\theta = 0$  case, the relationship (4.15) implies the agreement of not only the profile but also the overall normalization of the singular-value spectrum for  $U(N)$  and  $SU(N)$  at large  $N$ . Note, however, that the relationship (4.15) does not hold for nonzero  $\theta$ , which allows the appearance of the  $\theta$ -dependent overall factor for  $U(N)$  but not for  $SU(N)$ .

order to obtain the singular-value spectrum correctly up to a given  $D_{\text{cut}}$ . We have shown that this can be done efficiently by truncating the representations by their dimensionality using the fact that the totally symmetric representation gives the smallest dimensionality among the representations with the same  $l_1$ .

We have investigated the properties of the singular-value spectrum thus obtained in detail. In particular, we found that the spectrum has a definite profile in the large- $N$  limit up to an overall factor. This led us to a new interpretation of the Eguchi-Kawai reduction in the large- $N$  limit based on the self-similarity of the tensor network under the course-graining procedure. We also found an interesting change in the large- $N$  behavior of the spectrum in the  $U(N)$  case at the critical coupling of the Gross-Witten-Wadia phase transition. As a result, the singular-value spectrum obtained in the strong coupling phase becomes identical to that in the  $SU(N)$  case in the large- $N$  limit.

The singular values obtained up to large  $D_{\text{cut}}$  enabled us to obtain explicit results for finite  $N$  and finite  $V$ , and we discussed, in particular, how the Gross-Witten-Wadia third-order phase transition appears as  $N$  increases. We also investigated the  $U(N)$  gauge theory with the  $\theta$  term, and showed how the first-order phase transition at  $\theta = \pi$  associated with the spontaneous breaking of parity symmetry appears as the volume increases. In the large- $N$  limit, we observed a new type of volume independence for the topological charge in the strong coupling phase. We provided a theoretical understanding of this property by investigating the large- $N$  behavior of the singular-value spectrum in the presence of the  $\theta$  term. This volume independence goes beyond the Eguchi-Kawai reduction in that it refers to the  $O(1)$  term of the free energy. Whether this phenomenon occurs in large- $N$  gauge theories other than the ones considered in this paper is an interesting open question.

On the technical side, our work clearly shows that the TRG is indeed potentially useful in investigating  $SU(N)$  and  $U(N)$  gauge theories in general. However, we should also be aware of various technical complications that appear in applying the method to theories in higher dimensions and/or with matter fields. Note, in particular, that the singular values are determined not only by the representations but also by the internal degrees of freedom introduced by the Clebsch-Gordan coefficients [27]. The practical strategy to restrict the number of representations proposed in this paper is expected to be useful even in that case.

## Acknowledgements

We would like to thank D. Kadoh for valuable discussions. The computations were carried out on PC clusters in KEK Computing Research Center and KEK Theory Center.

# A Proof for the representation with the minimal dimensionality

In this section, we prove that the representation of the  $SU(N)$  group with the minimal dimensionality for a given  $l_1$  is the totally symmetric representation and its complex conjugate. Given that this fact plays a crucial role in our proposal for restricting the number of representations in Section 4.2, we provide the proof in an elementary fashion so that it is accessible to all the interested readers.

Let us recall that the representation of the  $SU(N)$  group is specified by (2.13) with an extra constraint  $l_N = 0$ , and the dimensionality  $d_r$  is given by (2.14). The statement is that  $d_r$  becomes minimum for a given  $l_1 = \Lambda$  when  $l_2 = \dots = l_{N-1} = 0$  or  $\Lambda$ , which we prove by induction.

Let us first take the log of (2.14) as

$$\log d_r = \sum_{1 \leq i < j \leq N} \log \left( 1 + \frac{l_i - l_j}{j - i} \right). \quad (\text{A.1})$$

We can easily check that the statement is true for the  $N = 3$  case, where we only have to minimize (A.1) with respect to  $l_2$  for fixed  $l_1 = \Lambda$  and  $l_3 = 0$ . We obtain

$$\log d_r = \log(\Lambda + 1 - l_2)(1 + l_2), \quad (\text{A.2})$$

which becomes minimum at  $l_2 = 0$  and  $\Lambda$ .

Next we assume that the statement is true for  $N$  and prove that it is true also for  $N + 1$ . The crucial point to note here is that the dimensionality  $d_r(N + 1)$  for the representation  $r = \{l_j\}$  ( $j = 1, \dots, N + 1$ ) of the  $SU(N + 1)$  group is given in terms of the dimensionality  $d_{\tilde{r}}(N)$  for the representation  $\tilde{r} = \{l_{j+1}\}$  ( $j = 1, \dots, N$ ) of the  $SU(N)$  group as

$$\log d_r(N + 1) = \log d_{\tilde{r}}(N) + \sum_{j=2}^N \log \left( 1 + \frac{\Lambda - l_j}{j - 1} \right) + \log \left( 1 + \frac{\Lambda}{N} \right). \quad (\text{A.3})$$

We minimize (A.3) in two steps. First we fix  $l_2 = \tilde{\Lambda}$  and minimize (A.3) within this constraint; then we minimize (A.3) with respect to  $\tilde{\Lambda}$ .

In the first step, we consider the first term and the second term separately. The first term is minimized when  $l_j = 0$  or  $\tilde{\Lambda}$  for  $2 \leq j \leq N$  by assumption. The second term is minimized when  $l_j = \tilde{\Lambda}$  ( $2 \leq j \leq N$ ). Thus we find that (A.3) is minimized when  $l_j = \tilde{\Lambda}$  ( $2 \leq j \leq N$ ) for fixed  $l_2 = \tilde{\Lambda}$ . Plugging this in (A.3), we obtain

$$\log d_r(N + 1) = \sum_{j=2}^N \log \left( 1 + \frac{\tilde{\Lambda}}{j - 1} \right) \left( 1 + \frac{\Lambda - \tilde{\Lambda}}{j - 1} \right). \quad (\text{A.4})$$

The second step is to minimize (A.4) with respect to  $\tilde{\Lambda}$ . Similarly to (A.2) for the SU(3) case, we find that each term in the sum appearing in (A.4) is minimized when  $\tilde{\Lambda} = 0$  or  $\Lambda$ . Thus we find that the statement is true for  $N + 1$ . This concludes the proof of the statement for arbitrary  $N$  by induction.

## References

- [1] M. Levin and C. P. Nave, *Tensor renormalization group approach to two-dimensional classical lattice models*, *Phys. Rev. Lett.* **99** (2007) [[cond-mat/0611687](#)].
- [2] G. Evenbly and G. Vidal, *Tensor network renormalization*, *Phys. Rev. Lett.* **115** (2015) [[1412.0732](#)].
- [3] J. F. Yu, Z. Y. Xie, Y. Meurice, Y. Liu, A. Denbleyker, H. Zou et al., *Tensor renormalization group study of classical xy model on the square lattice*, *Phys. Rev. E* **89** (2014) [[1309.4963](#)].
- [4] Z. Y. Xie, J. Chen, M. P. Qin, J. W. Zhu, L. P. Yang and T. Xiang, *Coarse-graining renormalization by higher-order singular value decomposition*, *Phys. Rev. B* **86** (2012) 045139 [[1201.1144](#)].
- [5] S. Wang, Z.-Y. Xie, J. Chen, B. Normand and T. Xiang, *Phase transitions of ferromagnetic potts models on the simple cubic lattice*, *Chin. Phys. Lett.* **31** (2014) 070503 [[1405.1179](#)].
- [6] Y. Shimizu, *Tensor renormalization group approach to a lattice boson model*, *Mod. Phys. Lett. A* **27** (2012) 1250035.
- [7] D. Kadoh, Y. Kuramashi, Y. Nakamura, R. Sakai, S. Takeda and Y. Yoshimura, *Tensor network analysis of critical coupling in two dimensional  $\phi^4$  theory*, *JHEP1905,184* (2019) [[1811.12376](#)].
- [8] Y. Shimizu and Y. Kuramashi, *Grassmann tensor renormalization group approach to one-flavor lattice schwinger model*, *Phys. Rev. D* **90** (2014) 014508 [[1403.0642](#)].
- [9] Y. Shimizu and Y. Kuramashi, *Critical behavior of the lattice schwinger model with a topological term at  $\theta = \pi$  using the grassmann tensor renormalization group*, *Phys. Rev. D* **90** (2014) 074503 [[1408.0897](#)].

- [10] S. Takeda and Y. Yoshimura, *Grassmann tensor renormalization group for the one-flavor lattice Gross–Neveu model with finite chemical potential*, *PTEP* **2015** (2015) 043B01 [1412.7855].
- [11] R. Sakai, S. Takeda and Y. Yoshimura, *Higher-order tensor renormalization group for relativistic fermion systems*, *PTEP* **2017** (2017) [1705.07764].
- [12] Y. Shimizu and Y. Kuramashi, *Berezinskii-kosterlitz-thouless transition in lattice schwinger model with one flavor of wilson fermion*, *Phys. Rev. D* **97** (2018) 034502 [1712.07808].
- [13] D. Kadoh, Y. Kuramashi, Y. Nakamura, R. Sakai, S. Takeda and Y. Yoshimura, *Tensor network formulation for two-dimensional lattice  $n = 1$  wess-zumino model*, *JHEP* **1803,141** (2018) [1801.04183].
- [14] Y. Yoshimura, Y. Kuramashi, Y. Nakamura, S. Takeda and R. Sakai, *Calculation of fermionic green functions with grassmann higher-order tensor renormalization group*, *Phys. Rev. D* **97** (2018) 054511 [1711.08121].
- [15] N. Butt, S. Catterall, Y. Meurice, R. Sakai and J. Unmuth-Yockey, *Tensor network formulation of the massless schwinger model with staggered fermions*, *Phys. Rev. D* **101** (2020) 094509 [1911.01285].
- [16] S. Akiyama and D. Kadoh, *More about the Grassmann tensor renormalization group*, 2005.07570.
- [17] S. Akiyama, Y. Kuramashi, T. Yamashita and Y. Yoshimura, *Restoration of chiral symmetry in cold and dense Nambu–Jona-Lasinio model with tensor renormalization group*, *JHEP* **01** (2021) 121 [2009.11583].
- [18] S. Akiyama and Y. Kuramashi, *Tensor renormalization group approach to  $(1 + 1)$ -dimensional hubbard model*, *Phys. Rev. D* **104** (2021) 014504 [2105.00372].
- [19] D. Adachi, T. Okubo and S. Todo, *Anisotropic tensor renormalization group*, 1906.02007.
- [20] D. Kadoh and K. Nakayama, *Renormalization group on a triad network*, 1912.02414.
- [21] S. Akiyama, Y. Kuramashi, T. Yamashita and Y. Yoshimura, *Phase transition of four-dimensional ising model with higher-order tensor renormalization group*, *Phys. Rev. D* **100** (2019) 054510 [1906.06060].

- [22] S. Akiyama, D. Kadoh, Y. Kuramashi, T. Yamashita and Y. Yoshimura, *Tensor renormalization group approach to four-dimensional complex  $\phi^4$  theory at finite density*, *JHEP* **09** (2020) 177 [2005.04645].
- [23] S. Akiyama, Y. Kuramashi and Y. Yoshimura, *Phase transition of four-dimensional lattice  $\phi^4$  theory with tensor renormalization group*, *Phys. Rev. D* **104** (2021) 034507 [2101.06953].
- [24] Y. Kuramashi and Y. Yoshimura, *Tensor renormalization group study of two-dimensional  $U(1)$  lattice gauge theory with a  $\theta$  term*, *JHEP* **04** (2020) 089 [1911.06480].
- [25] A. Bazavov, Y. Meurice, S.-W. Tsai, J. Unmuth-Yockey and J. Zhang, *Gauge-invariant implementation of the abelian-higgs model on optical lattices*, *Phys. Rev. D* **92** (2015) 076003 [1503.08354].
- [26] J. Unmuth-Yockey, J. Zhang, A. Bazavov, Y. Meurice and S.-W. Tsai, *Universal features of the abelian polyakov loop in 1 + 1 dimensions*, *Phys. Rev. D* **98** (2018) 094511 [1807.09186].
- [27] A. Bazavov, S. Catterall, R. G. Jha and J. Unmuth-Yockey, *Tensor renormalization group study of the non-abelian higgs model in two dimensions*, *Phys. Rev. D* **99** (2019) 114507 [1901.11443].
- [28] D. J. Gross and E. Witten, *Possible third-order phase transition in the large- $n$  lattice gauge theory*, *Phys. Rev. D* **21** (1980) 446.
- [29] S. R. Wadia,  *$n = \infty$  phase transition in a class of exactly soluble model lattice gauge theories*, *Phys. Lett. B* **93** (1980) 403.
- [30] B. E. Rusakov, *Loop averages and partition functions in  $u(n)$  gauge theory on two-dimensional manifolds*, *Mod. Phys. Lett. A* **05** (1990) 693.
- [31] T. Eguchi and H. Kawai, *Reduction of dynamical degrees of freedom in the large- $n$  gauge theory*, *Phys. Rev. Lett.* **48** (1982) 1063.
- [32] M. Fukuma, D. Kadoh and N. Matsumoto, *Tensor network approach to 2D Yang-Mills theories*, 2107.14149.
- [33] I. Bars and F. Green, *Complete integration of  $U(n)$  lattice gauge theory in a large- $n$  limit*, *Phys. Rev. D* **20** (1979) 3311.

- [34] I. Bars, *U(n) integral for the generating functional in lattice gauge theory*, *J. Math. Phys.* **21** (1980) 2678.
- [35] S. Samuel, *U(n) integrals, 1/n, and the de Wit–t hooft anomalies*, *J. Math. Phys.* **21** (1980) 2695 [<https://doi.org/10.1063/1.524386>].
- [36] J.-M. Drouffe and J.-B. Zuber, *Strong coupling and mean field methods in lattice gauge theories*, *Phys. Rep.* **102** (1983) 1.
- [37] G. Bhanot, U. M. Heller and H. Neuberger, *The quenched eguchi-kawai model*, *Phys. Lett. B* **113** (1982) 47.
- [38] R. Narayanan and H. Neuberger, *Large-n reduction in the continuum three-dimensional yang-mills theory*, *Phys. Rev. Lett.* **91** (2003) 081601 [[hep-lat/0303023](https://arxiv.org/abs/hep-lat/0303023)].
- [39] J. Kiskis, R. Narayanan and H. Neuberger, *Does the crossover from perturbative to nonperturbative physics in qcd become a phase transition at infinite n?*, *Phys. Lett. B* **574** (2003) 65 [[hep-lat/0308033](https://arxiv.org/abs/hep-lat/0308033)].
- [40] B. Fornberg, *Generation of finite difference formulas on arbitrarily spaced grids*, *Mathematics of Computation*, Vol. 51, No. 184 (1988) .
- [41] C. Bonati and P. Rossi, *Topological susceptibility of two-dimensional u(n) gauge theories*, *Phys. Rev. D* **99** (2019) 054503 [[1901.09830](https://arxiv.org/abs/1901.09830)].
- [42] C. Bonati and P. Rossi, *Topological effects in continuum two-dimensional u(n) gauge theories*, *Phys. Rev. D* **100** (2019) 054502 [[1908.07476](https://arxiv.org/abs/1908.07476)].
- [43] M. Hirasawa, A. Matsumoto, J. Nishimura and A. Yosprakob, *Complex Langevin analysis of 2D U(1) gauge theory on a torus with a  $\theta$  term*, *JHEP* **09** (2020) 023 [[2004.13982](https://arxiv.org/abs/2004.13982)].
- [44] C. Gattringer and O. Orasch, *Density of states approach for lattice gauge theory with a  $\theta$ -term*, *Nucl. Phys. B* **957** (2020) 115097.
- [45] J. M. Pawłowski, M. Scherzer, C. Schmidt, F. P. G. Ziegler and F. Ziesché, *Simulating yang-mills theories with a complex coupling*, *Phys. Rev. D* **103** (2021) 094505 [[2101.03938](https://arxiv.org/abs/2101.03938)].